A MATHEMATICAL MODEL FOR VORTEX-INDUCED OSCILLATION

BY

FRANCIS NGAI-HO LEE

B.A.Sc.,University of British Columbia, 1971.

A THESIS SUBMITTED IN PARTIAL FULFILMENT OF
THE REQUIREMENTS FOR THE DEGREE OF
MASTER OF APPLIED SCIENCE

in the Department
of
Mechanical Engineering

We accept this thesis as conforming to the
required standard.

THE UNIVERSITY OF BRITISH COLUMBIA

SEPTEMBER,1974

In presenting this thesis in partial fulfilment of the requirements for an advanced degree at the University of British Columbia, I agree that the Library shall make it freely available for reference and study. I further agree that permission for extensive copying of this thesis for scholarly purposes may be granted by the Head of my Department or by his representatives. It is understood that copying or publication of this thesis for financial gain shall not be allowed without my written permission.

Department of MECHANICAL ENGINEERING

The University of British Columbia
Vancouver 8, Canada

Date Sept. 30, 1974

Abstract

The flow around a circular cylinder exhibiting vortex-induced oscillation is modelled by 2 potential vortices in a 2-dimensional, inviscid and irrotational flow. The lift on the cylinder is obtained from the general form of the Blasius equation. Pressure distribution is obtained from the pressure equation in a moving frame of reference. The lift expression is coupled to the dynamic equation of the cylinder. The phase and amplitude of oscillation are determined by the method of equivalent linearization. A relationship between amplitude of oscillation and strength of the vortices is proposed. Root mean square pressure distribution at the Strouhal frequency on the surface of the oscillating cylinder is determined.

TABLE OF CONTENTS

LIST OF FIGURES

ACKNOWLEDGEMENT

The author would like to thank Dr. G. V. Parkinson for his advice and guidance in the course of this research.

The computing facilities of the Computing Center of the University of British Columbia were used to do the calculations involved in this reasearch.

LIST OF SYMBOLS

A, B	Positions of vortices in moving frame of reference
C_p	Fluctuating pressure coefficient
C_L	Lift coefficient
D	Drag
F	Complex potential
H	$=d/2a$
K	Vorticity shedding rate
L	Lift
M, N	Constants
P	$=c/2a$
S	Strouhal number
U	Free stream velocity
U	Cylinder velocity
$U_o - iU_c$	Complex velocity
V	$=U_o/2a\omega_n$
W	Cylinder complex velocity
Y	Non-dimensional cylinder displacement$=y/2a$
$\bar{Y}$	Non-dimensional amplitude$=\bar{y}/2a$
Z	Complex field variable
a	Radius of cylinder
$q, \bar{q}=c\pm id$	Positions of vortices in stationary frame of reference
f	External forcing function
f_v	Vortex formation frequency

f_1, f_2, f_3, f_4	Angles (see figure 6)
t	Time
m	Mass of cylinder per unit length
y_c	Cylinder displacement
$\bar{y}_c$	Amplitude of oscillation
β	Damping
θ	Angle
ω_n	Natural frequency of spring-cylinder system
ω_v	Vortex formation frequency in radians
ϕ	Velocity potential
ψ	Stream function
η	Mass parameter $=2a^2\rho/m$
τ	Non-dimensional time$=t\omega_n$
Φ	Phase angle
$\Gamma_o, \Gamma_L, \Gamma_u$	Circulations
α_o	Non-dimensional circulation $=\Gamma_o/U_o a$
Ω	Non-dimensional frequency $=\omega_v/\omega_n$
ρ	Fluid density

I Introduction

The phenomenon of wind-induced transverse oscillation of single bluff-shaped structures can be divided into two major categories according to the ways energy is extracted from the flow field. Galloping oscillation is the type of vibration caused by forces arising from the shape of the structure in the separated flow. With a small transverse disturbance velocity given to the structure, the two shear layers separating from the surface of the body interact with the body itself, generating a force in the same direction as the disturbance. Small disturbances therefore can grow into large amplitude oscillations. The other type of oscillation is the vortex-induced oscillation. The shear layers coming off from the surface of the structure at the separation points are unstable to small disturbances in the flow field. They tend to roll up into large discrete vortices. These large discrete vortices are created alternately from both shear layers, forming the well-known Karman vortex street. These vortices induce alternating pressure loading on the surface of the structure. When the vortex formation frequency is in the neighborhood of any of the natural frequencies of a lightly-damped structure, the structure would be excited into resonant oscillation.

The subject of vortex-induced oscillation has been under investigation since 1878 by different researchers in different parts of the world. A tremendous amount of data has been accumulated. It has been known that vortex-induced oscillation is not a simple cause-and-effect phenomenon. There is an interdependence between the force that causes the structure to oscillate and the oscillation. Naudascher (1) and Toebes (2) have recognized this fact and termed it fluid-elastic interaction. However, without some kind of analytic model, the interplay between the different physical quantities involved in the phenomenon cannot be adequately established. Engineering attempts either to make use of or to eliminate the phenomena of vortex-induced oscillation would benefit from a successful mathematical description of the phenomena. Furthermore, a deeper insight could be gained into the physics of the flow.

The search for a proper mathematical model has already begun. As in experimental work, the most widely studied bluff shape is the circular cylinder. Since all Newtonian fluid flow phenomena are governed by the Navier-Stokes equations, an obvious approach to this problem is to solve the full Navier-Stokes equations for the flow field in the presence of the oscillating circular cylinder. Because of the complexity of this system of equations, no such solution has been found. With some simplification, Jordan and Fromm (6) have developed computer programs to solve the Navier-Stokes equations for the time-dependent, viscous and incompressible flow past a stationary circular cylinder. They obtained results for lift, drag, torque and pressure distribution on the cylinder at 3 Reynolds numbers (Rn) of 100, 400 and 1000. Results for the first two are in good agreement with experimental results, while for the third one, significant discrepancies were found because of the difficulty encountered in modelling the thin boundary layer upstream of the separation point, and the 3-dimensional nature of the flow.

Because of the complexity of the Navier-Stokes equations, simpler models would seem to be a better approach from an analytic point of view. Potential flow models are appealing in this respect because of the simpler but elegant mathematical theory that has been developed. If one looks at a separated flow, the important entities involved are the thin shear layers and the discrete vortices. With these in mind, Gerrard (7), Abernathy and Kronauer (8) and others have studied two-dimensional potential models of stationary circular cylinders in uniform flow. In their models, the thin shear layers are modelled as sheets of discrete point vortices. They have shown, by use of lengthy computer programs, that the vortex sheets do roll up to form large clusters of vortices at the observed positions of actual discrete vortices behind the circular cylinder with circulation strengths that agree with experimental ones. They also obtained values for the forces on the stationary cylinder in good agreement with the measured ones

One disappointing drawback of these models is that important analytic relationships between the principal quantities are masked in fine numerical details. They do not throw much light on the physics of the phenomena. Yet simpler models are required. A single-vortex model (see figure 1) was proposed by Etkin, and McGregor (9) used it to obtain pressure distributions on the surface of a stationary cylinder. As shown in figure 1, the root mean square (RMS) of the fluctuating pressure coefficient at the Strouhal frequency obtained from this model agrees fairly well with the ones he measured over the front portion of the cylinder.

A logical extension of this model would be to have two such potential vortices located on either side of the wake centerline (see figure 2). Madderom (10) applied this model to obtain the RMS of the fluctuating pressure coefficient at the Strouhal frequency on a stationary circular cylinder. As can be seen from figure 2, the agreement is better than for Etkin's single-vortex model.

In the stationary-cylinder models mentioned above, only the flow field needs to be modelled. For vortex-induced oscillation of a bluff cylinder, this is only half of the problem. The dynamics of the oscillating cylinder must also be dealt with. Several dynamic models for the oscillation of a circular cylinder have been proposed. These models often lump the effect of the wake into some kind of oscillator which generates the lift on the cylinder. A promising and more successful one was proposed by Hartlen and Currie (11). In their model, lift is governed by a non-linear differential equation coupled to the velocity of oscillation linearly. This model was able to predict most of the characteristics of vortex-induced oscillation fairly well.

None of the models mentioned so far take both the dynamics of the flow field and the oscillating body into account. It is felt that perhaps a better understanding of vortex-induced oscillation can be gained if we couple Madderom's flow field model, because of its ability to predict the pressure distribution in the static case and its realistic simplicity and analytic tractability, to the dynamic equation governing the motion of the circular cylinder. It is to this end this research has been aimed.

II Formulation of the Mathematical Model

i) Experimental Observations

A very comprehensive experimental study of vortex-induced oscillation in both circular and D-section cylinders was carried out in this laboratory by C. C. Feng (3) at Reynolds numbers in the neighborhood of 2×10^4. His findings show that vortex-induced oscillation of a circular cylinder is sinusoidal in time t so that the displacement y_c can be expressed by

$$y_c = \bar{y}_c \sin(\omega_n t + \bar{\Phi}) \qquad (1)$$

where $\bar{y}_c$ is the amplitude, ω_n the natural frequency of the spring-cylinder system he used, $\bar{\Phi}$ the phase angle measured relative to excitation. He found hysteresis loops exist in both amplitude and phase. As shown in the $\bar{Y}$ vs V curve in figure 3, where $\bar{Y} = \bar{y}_c/2a$ is the non-dimensional amplitude and $V = U_0/2a\omega_n$ is the non-dimensional velocity, U_0 being the free stream velocity, starting from A, if we increase the flow velocity V, amplitude increases accordingly to B. However, further increase in velocity beyond B would result in a sudden drop in amplitude, to C. The amplitude will then diminish slowly to D. If we start from D and decrease the flow velocity, amplitude will increase slowly, through C to E. Further decrease will make the amplitude jump from E to F. It will then decrease with velocity to A.

Phase measurements show the same kind of jump as shown in figure 3.

It is well known that vortex formation frequency f_v in the wake of a bluff body is governed by the Strouhal relationship

$$f_v = S\frac{U_0}{2a} \tag{2}$$

where S is the Strouhal number and a is the radius of the cylinder. If we look at the ratio ω_v/ω_n in figure 3, where $\omega_v = 2\pi f_v$, as a function of velocity, starting at the neighborhood of V=.8, instead of following the Strouhal relationship, the vortex formation frequency is the same as the natural frequency of the cylinder-spring system for a range of velocities up to V=1.1. It looks as though the vortex formation frequency is locked into the natural frequency of the system. This range of velocity is known as the lock-in range. The frequency reverts back to the Strouhal frequency beyond V=1.1

ii) Derivation of the Complex Potential

With the set-up shown in figure 4, we have in the complex Z-plane, a circular cylinder of radius a, free to move in the y-direction in a uniform, 2-dimensional, inviscid and irrotational flow with free stream velocity U_0. Located downstream of the cylinder are two potential vortices at points ξ, $\bar{\xi}=c\pm id$. The strengths of these vortices are given by $\Gamma_u=\Gamma_0(M+N\cos\omega_v t)$ at ξ and $\Gamma_L=\Gamma_0(M-N\cos\omega_v t)$ at $\bar{\xi}$. M and N are positive constants such that M>N and M+N=1. Γ_0 is the effective circulation. In their laboratory studies, Feng (3), Koopmann (4) and Gerrard (5) all observed that when the cylinder was stationary or oscillating with low amplitude, the vortex filament coming off the surface of the cylinder was inclined at an angle to the axis of the cylinder. When the cylinder was exhibiting maximum amplitude of oscillation, the vortex filament was aligned parallel to the axis of the cylinder. This is a 3-dimensional effect which a 2-dimensional model like this is unable to include. Therefore it is assumed that $\Gamma_0=\Gamma_0(\bar{Y})$ and the form of the function remains to be determined.

The complex potential F(Z) for the cylinder-vortex system as shown in figure 4 with $y_c=0$ in a flow with arbitrary complex velocity (U_0+iU_c) in the complex plane is given by

$$F(z)=\phi+i\psi=(U_0+iU_c)z+(U_0-iU_c)\frac{a^2}{z}$$

$$+i\frac{\Gamma_u}{2\pi}\ln(z-\xi)-i\frac{\Gamma_u}{2\pi}\ln\left(\frac{a^2}{z}-\bar{\xi}\right)$$

$$-i\frac{\Gamma_L}{2\pi}\ln(z-\bar{\xi})+i\frac{\Gamma_L}{2\pi}\ln\left(\frac{a^2}{z}-\xi\right)$$

where ϕ is the velocity potential and ψ is the stream function. Now if we impose a complex velocity $-(U_0+iU_c)$ on the whole system, i.e. stopping the on-coming flow and setting the cylinder-vortex system into motion with complex velocity $-(U_0+iU_c)$, the complex potential becomes

$$F(z)=\phi+i\psi=(U_0-iU_c)\frac{a^2}{z}+i\frac{\Gamma_u}{2\pi}\ln(z-\zeta)$$

$$-i\frac{\Gamma_u}{2\pi}\ln\left(\frac{a^2}{z}-\bar{\zeta}\right)-\frac{i\Gamma_L}{2\pi}\ln(z-\bar{\zeta})$$

$$+i\frac{\Gamma_L}{2\pi}\ln\left(\frac{a^2}{z}-\zeta\right)$$

Finally the two vortices are given a motion that would stop them from moving in the y-direction. This will show up in the position of the vortices relative to the cylinder. The complex potential becomes

$$F(z)=\phi+i\psi=(U_0-iU_c)\frac{a^2}{z}+i\frac{\Gamma_u}{2\pi}\ln(z-A)$$

$$-i\frac{\Gamma_u}{2\pi}\ln\left(\frac{a^2}{z}-\bar{A}\right)-i\frac{\Gamma_L}{2\pi}\ln(z-B)$$

$$+i\frac{\Gamma_L}{2\pi}\ln\left(\frac{a^2}{z}-\bar{B}\right)$$

in which $A=\zeta-iy_c$, $B=\bar{\zeta}-iy_c$, y_c is the displacement of the cylinder with respect to the fixed frame of reference $Z=(x+iy)$.

Neglecting some constants, $F(Z)$ can be simplified to

$$F(z)=(U_0-iU_c)\frac{a^2}{z}+i\frac{\Gamma_u}{2\pi}\left\{\ln(z-A)-\ln\left(z-\frac{a^2}{\bar{A}}\right)\right\}$$

$$+i\frac{\Gamma_L}{2\pi}\left\{\ln\left(z-\frac{a^2}{\bar{B}}\right)-\ln(z-B)\right\} \qquad (3)$$

iii) Lift and Drag Equation

By potential flow theory, the complex velocity ($U-iV_c$) can be obtained by differentiating the complex potential with respect to the field variable Z. Therefore

$$U-iV_c = \frac{dF}{dz} = -(U_0 - iU_c)\frac{a^2}{z^2} + i\frac{\Gamma_U}{2\pi}\left\{\frac{1}{(z-A)} - \frac{1}{(z-\frac{a^2}{\bar{A}})}\right\}$$

$$+ i\frac{\Gamma_L}{2\pi}\left\{\frac{1}{(z-\frac{a^2}{\bar{B}})} - \frac{1}{(z-B)}\right\} \qquad (4)$$

from the general form of the Blasius equation, (see 12, page 255) the lift L and drag D on a moving cylinder are given by

$$D-iL = \frac{1}{2}i\rho\oint_c \left(\frac{dF}{dz}\right)^2 dz + i\rho\frac{\partial}{\partial t}\oint_c \bar{F}(\bar{z})d\bar{z}$$

$$+ i\rho\Gamma W + \rho A_c \frac{dW}{dt}$$

$$= I_1 + I_2 + i\rho\Gamma W + \rho A_c \frac{dW}{dt} \qquad (5)$$

where ρ is the fluid density, Γ the total circulation inside the cylinder, $W=-U_0-iU_c$, the complex velocity of the cylinder, and A_c the cross-sectional area of the cylinder. The C at the bottom of the integral sign denotes a contour integral along the surface of the cylinder. We will now consider the two integrals I_1 and I_2 .

From equation (4), we obtained $(\frac{dF}{dz})^2$ and

$$\frac{i}{2}\rho\oint_c (\frac{dF}{dz})^2 dz = \frac{i}{2}\rho\oint_c \Big\{ [(U_0 - iU_c)\frac{a^2}{z^2}]^2 + [\frac{i\Gamma_U}{2\pi}\frac{1}{(z-A)}]^2$$

$$+ [\frac{i\Gamma_U}{2\pi}\frac{1}{(z-\frac{a^2}{A})}]^2 + [\frac{i\Gamma_L}{2\pi}\frac{1}{(z-\frac{a^2}{B})}]^2 + [\frac{i\Gamma_L}{2\pi}\frac{1}{(z-B)}]^2$$

$$+ \frac{\Gamma_U^2}{2\pi^2}\frac{1}{(z-A)(z-\frac{a^2}{A})} + \frac{\Gamma_L^2}{2\pi^2}\frac{1}{(z-B)(z-\frac{a^2}{B})}$$

$$- (U_0 - iU_c)\frac{a^2}{z}[\frac{i\Gamma_U}{\pi}(\frac{1}{(z-A)} - \frac{1}{(z-\frac{a^2}{A})}) + \frac{i\Gamma_L}{\pi}(\frac{1}{z-\frac{a^2}{B}} - \frac{1}{z-B})$$

$$- \frac{\Gamma_U\Gamma_L}{2\pi^2}[\frac{1}{z-A} - \frac{1}{z-\frac{a^2}{A}}][\frac{1}{z-\frac{a^2}{B}} - \frac{1}{z-B}] \Big\} dz$$

By using the method of residues, this integral can be easily evaluated. The final result is

$$\frac{i}{2}\rho\oint_c (\frac{dF}{dz})^2 dz = -\pi\rho\Big\{\frac{\Gamma_U^2}{2\pi^2}\frac{1}{(\frac{a^2}{A}-A)} + \frac{\Gamma_L^2}{2\pi^2}\frac{1}{(\frac{a^2}{B}-B)} + \frac{i\Gamma_U(U_0-iU_c)a^2}{\pi A^2}$$

$$- \frac{i\Gamma_L(U_0-iU_c)a^2}{\pi B^2} - \frac{\Gamma_U\Gamma_L}{2\pi^2}(\frac{1}{\frac{a^2}{A}-B} + \frac{1}{\frac{a^2}{B}-A})\Big\} \qquad (6)$$

Separating this into the real and imaginary parts, we obtain

$$\frac{i}{2}\rho\oint_c (\frac{dF}{dz})^2 dz = \rho\Big\{-\frac{\Gamma_U^2}{2\pi}\frac{c}{(a^2-|A|^2)} - \frac{\Gamma_L^2}{2\pi}\frac{c}{(a^2-|B|^2)}$$

$$- \Gamma_U\frac{[U_c a^2[c^2-(y_c-d)^2] - 2U_0 c a^2(y_c-d)]}{|A|^4}$$

$$+ \Gamma_L\frac{[U_c a^2[c^2-(y_c+d)^2] - 2U_0 c a^2(y_c+d)]}{|B|^4}$$

$$+ \frac{\Gamma_U \Gamma_L}{\pi} \frac{c\,[c^2 + y_c^2 - d^2]}{[c^2 + y_c^2 - d^2]^2 + 4d^2c^2} \Big\} - i\rho \Big\{ \frac{\Gamma_U^2}{2\pi} \frac{(y_c - d)}{a^2 - |A|^2}$$

$$+ \frac{\Gamma_L^2}{2\pi} \frac{(y_c + d)}{a^2 - |B|^2} - \frac{\Gamma_U \Gamma_L}{\pi} \frac{y_c\,(c^2 + y_c^2 - d^2)}{(c^2 + y_c^2 - d^2)^2 + 4c^2d^2}$$

$$+ \frac{2\Gamma_U u_c c a^2 (y_c - d) + a^2 u_0 \Gamma_U \,[c^2 - (y_c - d)^2]}{|A|^4}$$

$$- \frac{\Gamma_L a^2 u_0 \,[c^2 - (y_c + d)^2] + 2\Gamma_L u_c c a^2 (y_c + d)}{|B|^4} \Big\} \qquad (7)$$

where $|A|$ and $|B|$ are the absolute values of A and B.

Now we turn our attention to I_2 in equation (5). The integral that we have to evaluate is

$$i\rho \frac{\partial}{\partial t} \oint_c \bar{F}(\bar{z})\,d\bar{z} = i\rho \frac{\partial}{\partial t} \oint_c \overline{F(z)\,dz}$$

$$= i\rho \frac{\partial}{\partial t} \oint_c \overline{\Big\{ (u_0 - iu_c)\frac{a^2}{z} + \frac{i\Gamma_U}{2\pi} \big[\ln(z - A) - \ln(z - \tfrac{a^2}{\bar{A}})\big]}$$

$$\overline{+ \frac{i\Gamma_L}{2\pi} \big[\ln(z - \tfrac{a^2}{\bar{B}}) - \ln(z - B)\big] \Big\}\, dz} \qquad (8)$$

The first term can be evaluated readily by the method of residues and

$$\oint_c (u_0 - iu_c)\frac{a^2}{z}\,dz = 2\pi i\,(u_0 - iu_c)\,a^2$$

However, the second term involves, instead of a singularity, two branch points at $Z=A$ and $Z=a^2/\bar{A}$. Since $Z=A$ is outside the cylinder, it does not have any contribution. The only branch point we have to consider is $Z=a^2/\bar{A}$, the inverse point of A.

Taking a branch cut as shown in figure (5A), we deform the contour of integration as indicated by the arrows. By Cauchy's theorem,

$$\int_{r\to s} + \int_{s\to t} + \int_{t\to u} + \int_{u\to r} = 0$$

$$\therefore \int_{r\to s} = -\left\{ \int_{s\to t} + \int_{t\to u} + \int_{u\to r} \right\}$$

In the limit $\epsilon \to 0$,

$$\lim_{\epsilon\to 0} \int_{r\to s} = \oint_c = -\left\{ \int_{s\to t} + \int_{t\to u} + \int_{u\to r} \right\} \qquad (9)$$

First consider the line integral from $s \to t$. Let

$$z - \frac{a^2}{\bar{A}} = \varsigma e^{i\gamma}$$

$$\therefore dz = i\varsigma e^{i\gamma} d\gamma + e^{i\gamma} d\varsigma$$

$$\ln\left(z - \frac{a^2}{\bar{A}}\right) = \ln \varsigma + i\gamma$$

Along the path $s \to t$, γ = constant = γ_u and ς varies from $\varsigma = (a - \frac{a^2}{|A|})$ at s to $\varsigma = 0$ at t. $dz = e^{i\gamma} d\varsigma$.

$$\therefore \int_{s\to t} \ln\left(z - \frac{a^2}{\bar{A}}\right) dz = \int_{(a-\frac{a^2}{|A|})}^{0} (\ln\varsigma + i\gamma_u) e^{i\gamma_u} d\varsigma$$

$$= e^{i\gamma_u}\left[-\left(a - \frac{a^2}{|A|}\right)\ln\left(a^2 - \frac{a^2}{|A|}\right) + \left(a - \frac{a^2}{|A|}\right) - i\gamma_u\left(a - \frac{a^2}{|A|}\right)\right]$$

Along the path $t \to u$, ς = constant= ε as we chose it to be so when we chose the path of integration. γ varies from $\gamma = \gamma_u$ at t to $\gamma = -2\pi + \gamma_u$ at u. $dz = i\varsigma e^{i\gamma} d\gamma$.

$$\therefore \int_{t \to u} \ln\left(z - \frac{a^2}{\bar{A}}\right) dz = \int_{\gamma_u}^{-2\pi + \gamma_u} (\ln\varsigma + i\gamma)\, i\varsigma e^{i\gamma} d\gamma$$

As $\varepsilon \to 0$, $\ln\varsigma \to \infty$ and $\varsigma \to 0$. But $\varsigma \to 0$ faster than $\ln\varsigma \to \infty$. Therefore we can say the integral is zero.

Along the path $u \to r$, γ = constant= $-2\pi + \gamma_u$ and ς varies from zero at u to $(a - \frac{a^2}{|\bar{A}|})$ at r. $dz = e^{i\gamma} d\varsigma$.

$$\therefore \int_{u \to r} \ln\left(z - \frac{a^2}{\bar{A}}\right) dz = \int_0^{(a - \frac{a^2}{|\bar{A}|})} (\ln\varsigma + i\gamma) e^{i\gamma} d\varsigma$$

$$= e^{i\gamma_u}\left\{\left(a - \frac{a^2}{|\bar{A}|}\right)\ln\left(a - \frac{a^2}{|\bar{A}|}\right) - \left(a - \frac{a^2}{|\bar{A}|}\right) + i(-2\pi + \gamma_u)\left(a - \frac{a^2}{|\bar{A}|}\right)\right\}$$

Putting the results back into equation (9), we obtain

$$\oint_c \ln\left(z - \frac{a^2}{\bar{A}}\right) dz = e^{i\gamma_u}\left[2\pi i\left(a - \frac{a^2}{|\bar{A}|}\right)\right]$$

For the third term in equation (8), the branch point of interest is $z = a^2/\bar{B}$. We choose our branch cut as shown in figure (5B). Following the same procedure, the integral is found to be

$$\oint_c \ln\left(z - \frac{a^2}{\bar{B}}\right) dz = 2\pi i\, e^{-i\gamma_L}\left(a - \frac{a^2}{|B|}\right)$$

and equation (8) becomes

$$i\rho \frac{\partial}{\partial t} \oint_c \overline{\left\{ (u_0 + i u_c)\frac{a^2}{z} + i\frac{\Gamma_U}{2\pi}\left[\ln(z - A) - \ln\left(z - \frac{a^2}{\bar{A}}\right)\right]\right.}$$

$$\overline{\left. + i\frac{\Gamma_L}{2\pi}\left[\ln\left(z - \frac{a^2}{\bar{B}}\right) - \ln(z - B)\right]\right.} dz$$

$$= i\rho\frac{\partial}{\partial t}\left\{ -2\pi i (u_0 + i u_c) a^2 + \Gamma_U\left(a - \frac{a^2}{|A|}\right)e^{-i\gamma_U} - \Gamma_L\left(a - \frac{a^2}{|B|}\right)e^{i\gamma_L}\right\}$$

This expression can be separated into its real and imaginary parts,

$$= \rho\frac{\partial}{\partial t}\left\{ 2\pi u_0 a^2 + \Gamma_U\left(a - \frac{a^2}{|A|}\right)\sin\gamma_U + \Gamma_L\left(a - \frac{a^2}{|B|}\right)\sin\gamma_L\right\}$$

$$+ i\rho\frac{\partial}{\partial t}\left\{ 2\pi u_c a^2 + \Gamma_U\left(a - \frac{a^2}{|A|}\right)\cos\gamma_U - \Gamma_L\left(a - \frac{a^2}{|B|}\right)\cos\gamma_L\right\} \qquad (10)$$

The remaining two terms in equation (5) can be evaluated quite readily.

$$i\rho\Gamma w = i\rho\,(-\Gamma_U + \Gamma_L)(-u_0 + i u_c) \qquad (11)$$

$$\rho A_c \frac{dw}{dt} = \rho\pi a^2\left(i\frac{du_c}{dt}\right) \qquad (12)$$

With the results in equations (7), (10), (11), and (12) substituted back into equation (5), we obtain

$$D - iL = \rho\Big\{-\frac{\Gamma_u^2}{2\pi}\frac{c}{(a^2-|A|^2)} - \frac{\Gamma_L^2}{2\pi}\frac{c}{(a^2-|B|^2)} - \frac{\Gamma_u a^2[u_c[c^2-(y_c-d)^2]-2cU_o(y_c-d)}{|A|^4}$$

$$\frac{\Gamma_L a^2[U_c[c^2-(y_c+d)^2]-2U_o c(y_c+d)]}{|B|^4} + \frac{\Gamma_u\Gamma_L}{\pi}\frac{c(c^2+y_c^2-d^2)}{(c^2+y_c^2-d^2)^2+4d^2c^2}\Big\}$$

$$+\frac{\partial}{\partial t}\Big\{2\pi u_o a^2 + \Gamma_u(a-\frac{a^2}{|\bar{A}|})\sin\gamma_u + \Gamma_L(a-\frac{a^2}{|\bar{B}|})\sin\gamma_L\Big\} + U_c(\Gamma_L-\Gamma_u)$$

$$-i\rho\Big\{\frac{\Gamma_u^2}{2\pi}\frac{(y_c-d)}{a^2-|A|^2} + \frac{\Gamma_L^2}{2\pi}\frac{(y_c+d)}{a^2-|B|^2} + \frac{2\Gamma_u U_c c a^2(y_c-d)+a^2U_o\Gamma_u[c^2-(y_c-d)^2]}{|A|^4}$$

$$-\frac{\Gamma_L a^2 U_o[c^2-(y_c+d)^2]+2\Gamma_L U_c c a^2(y_c+d)}{|B|^4} - \frac{\Gamma_u\Gamma_L}{\pi}\frac{c[c^2+y_c^2-d^2]}{(c^2+y_c^2-d^2)^2+4d^2c^2}$$

$$-\frac{\partial}{\partial t}\Big[2\pi U_c a^2 + \Gamma_u(a-\frac{a^2}{|\bar{A}|})\cos\gamma_u - \Gamma_L(a-\frac{a^2}{|\bar{B}|})\cos\gamma_L\Big] + U_o(\Gamma_L-\Gamma_u)$$

$$-\pi a^2\frac{dU_c}{dt}\Big\} \qquad (13)$$

We define a lift coefficient C_L in the conventional way and $C_L = L/\rho u_o^2 a$. Furthermore, all quantities involved are non-dimensionalized according to the following scheme:

(1) Circulation is non-dimensionalized with $U_o a$

(2) Length is non-dimensionalized with 2a.

(3) Time is non-dimensionalized with ω_n.

(4) Frequency is non-dimensionalized with ω_n.

(5) Velocity is non-dimensionalized with $2a\omega_n$.

The following expression for C_L is obtained:

$$C_L = \frac{\alpha_u^2}{\pi}\frac{(Y-H)}{[1-4\{(Y-H)^2+P^2\}]} + \frac{\alpha_L^2}{\pi}\frac{(Y+H)}{[1-4\{(Y+H)^2+P^2\}]}$$

$$+\alpha_u\left\{\frac{2\dot{Y}(Y-H)P + V[P^2-(Y-H)^2] - 2(Y-H)[(H-Y)^2+P^2]^{1/2}P\dot{Y}}{4V[(Y-H)^2+P^2]^2} - 1\right\}$$

$$-\alpha_L\left\{\frac{2\dot{Y}(Y+H)P + V[P^2-(Y+H)^2] - 2(Y+H)[(H-Y)^2+P^2]^{1/2}P\dot{Y}}{4V[(Y+H)^2+P^2]^2} - 1\right\}$$

$$-\frac{\dot{\alpha}_u\pi S P[\{(Y-H)^2+P^2\}^{1/2}-1/2]}{(Y-H)^2+P^2} + \frac{\dot{\alpha}_L\pi S P[\{(Y+H)^2+P^2\}^{1/2}-1/2]}{(Y+H)^2+P^2}$$

$$-\frac{\alpha_u\alpha_L}{2\pi}\frac{(P^2+Y^2-H^2)Y}{(P^2-H^2+Y^2)^2+4P^2H^2} - \frac{3}{2}\pi\frac{\ddot{Y}}{V^2} \qquad (14)$$

where $Y = y_c/2a$, $H = d/2a$, $P = c/2a$, $V = U_0/2a\omega_n$, $S = a\omega_n/\pi U_0$ is the Strouhal number and $\alpha_{u,L} = \Gamma_{u,L}/U_0 a$. Dot represents differentiation with respect to the dimensionless time $\tau = t\omega_n$.

iv) Pressure Equation

In a moving frame of reference, the pressure P at any point in the field is given by (see 12 page 252)

$$p = p_\infty - \rho\frac{\partial\phi}{\partial t} - \frac{\rho}{2}e^{2i\alpha}\left[\frac{dF(z)}{dz} - w\right]^2 + \frac{\rho}{2}|w|^2$$

Where p_∞ is the pressure at infinity, ϕ the velocity potential as defined in equation(3), α the angle shown in figure 6. A pressure coefficient can be defined in the conventional way, i.e.

$$C_p = \frac{P - P_\infty}{\frac{1}{2}\rho U_0^2} = -\frac{2}{U_0^2}\frac{\partial\phi}{\partial t} - \frac{e^{2i\alpha}}{U_0^2}\left[\frac{dF}{dz} - W\right]^2 + \frac{|W|^2}{U_0^2}$$

On the surface of the cylinder, $Z = a\cos\theta + ia\sin\theta$ and ϕ is obtained there from the real part of equation (3)

$$\phi = a(U_0\cos\theta - U_c\sin\theta) + \frac{T_U}{2\pi}(f_1 - f_2) + \frac{T_L}{2\pi}(f_3 - f_4)$$

where θ, f_1, f_2, f_3 and f_4 are shown in figure 6.

$$C_p = 1 + \left(\frac{U_c}{U_0}\right)^2 - \frac{1}{U_0^2}\left[\frac{T_U'}{\pi}(f_1 - f_2) + \frac{T_L'}{\pi}(f_3 - f_4) + \frac{T_U}{\pi}(f_1' - f_2')\right.$$

$$\left. + \frac{T_L}{\pi}(f_3' - f_4') - 2aU_c'\sin\theta\right] + \frac{[\cos 2\theta + i\sin 2\theta]}{U_0^2} \times$$

$$\left\{-U_0\cos 2\theta + U_c\sin 2\theta + iU_0\cos 2\theta + iU_0\sin 2\theta + \frac{iT_U}{2\pi} \times\right.$$

$$\left[\frac{(a\cos\theta - c) - i\{a\sin\theta - (d - y_c)\}}{(a\cos\theta - c)^2 + (a\sin\theta - d + y_c)^2} - \{c - i(d - y_c)\} \times\right.$$

$$\left.\frac{\{-a^2 + a\cos\theta c + a\sin\theta(d - y_c) - i[ca\sin\theta - (d - y_c)a\cos\theta]\}}{\{-a^2 + ca\cos\theta + a(d - y_c)\sin\theta\}^2 + \{ca\sin\theta - (d - y_c)a\cos\theta\}^2}\right]$$

$$+\frac{i\Gamma_L}{2\pi}\left[\frac{\{c+i(d-y_c)\}\left(\{ca\cos\theta-(d+y_c)a\sin\theta-a^2\}-i[ca\sin\theta+(d+y_c)a\cos\theta]\right)}{[ca\cos\theta-a\sin\theta(d+y_c)-a^2]^2+[ca\sin\theta+(d+y_c)a\cos\theta]^2}\right.$$

$$\left.-\frac{(a\cos\theta-c)-i(a\sin\theta+d+y_c)}{(a\cos\theta-c)^2+(a\sin\theta+y_c+d)^2}\right]+u_0+iu_c\Big\}^2$$

Where prime indicates differentiating with respect tc time t. With some lengthy and tedious algebra, this expression can be simplified to the following:

$$C_p = 1+\frac{u_c^2}{u_0^2}-\frac{1}{u_0^2}\Big[\frac{\Gamma_u'}{\pi}(f_1-f_2)+\frac{\Gamma_L'}{\pi}(f_3-f_4)+\frac{\Gamma_u}{\pi}(f_1'-f_2')$$

$$+\frac{\Gamma_L}{\pi}(f_3'-f_4')-2au_c'\sin\theta\Big]+2(\cos 2\theta-1)-2\frac{u_c^2}{u_0^2}(\cos 2\theta+1)$$

$$-4\frac{u_c}{u_0}\sin 2\theta-2K_0\left(2\sin\theta+4\frac{u_c}{u_0}\cos\theta\right)-K_0^2 \qquad (15)$$

where $f_1 = \tan^{-1}\left\{\frac{a\sin\theta-a^2\sin\psi_1/[c^2+(d-y_c)^2]^{1/2}}{a\cos\theta-a^2\cos\psi_1/[c^2+(d-y_c)^2]^{1/2}}\right\}$

$$f_2 = \tan^{-1}\left\{\frac{a\sin\theta+y_c-d}{a\cos\theta-c}\right\}$$

$$f_3 = \tan^{-1}\left\{\frac{a\sin\theta+y_c+d}{a\cos\theta-c}\right\}$$

$$f_4 = \tan^{-1}\left\{\frac{a\sin\theta-a^2\sin\psi_2/[c^2+(d+y_c)^2]^{1/2}}{a\cos\theta-a^2\cos\psi_2/[c^2+(d+y_c)^2]^{1/2}}\right\}$$

$$K_o = \frac{\alpha_u}{2\pi} \frac{1 - [c^2 + (d-y_c)^2]/a^2}{[1 + \frac{(d-y_c)^2 + c^2}{a^2} - 2(\cos\theta \frac{c}{a} + \sin\theta \, (\frac{d-y_c}{a}))]}$$

$$- \frac{\alpha_L}{2\pi} \frac{1 - [c^2 + (d+y_c)^2]/a^2}{[1 + \frac{c^2 + (d+y_c)^2}{a^2} - 2(\cos\theta \frac{c}{a} - \sin\theta \, \frac{(d+y_c)}{a})]}$$

$$f_1' = \left\{ \left[\frac{-a^2 \cos\psi_1 \frac{d\psi_1}{dt}}{\{c^2 + (d-y_c)^2\}^{1/2}} - \frac{a^2 \sin\psi_1 (d-y_c) \frac{dy_c}{dt}}{\{c^2 + (d-y_c)^2\}^{3/2}} \right] \left[a\cos\theta - \frac{a^2 \cos\psi_1}{\{c^2 + (d-y_c)^2\}^{1/2}} \right] \right.$$

$$\left. - \left[a\sin\theta - \frac{a^2 \sin\psi_1}{\{c^2 + (d-y_c)^2\}^{1/2}} \right] \left[\frac{a^2 \sin\psi_1 \frac{d\psi_1}{dt}}{\{c^2 + (d-y_c)^2\}^{1/2}} - \frac{(d-y_c) \frac{dy_c}{dt} a^2 \cos\psi_1}{[c^2 + (d-y_c)^2]^{3/2}} \right] \right\} \Big/$$

$$\left\{ \left[a\cos\theta - \frac{a^2 \cos\psi_1}{\{c^2 + (d-y_c)^2\}^{1/2}} \right]^2 + \left[a\sin\theta - \frac{a^2 \sin\psi_1}{\{c^2 + (d-y)^2\}^{1/2}} \right]^2 \right\}$$

$$f_2' = \left\{ \frac{dy_c}{dt} \Big/ (a\cos\theta - c) \right\} \Big/ \left\{ 1 + \left(\frac{a\sin\theta + y_c - d}{a\cos\theta - c} \right) \right\}^2$$

$$f_3' = \left\{ \frac{dy_c}{dt} \Big/ (a\cos\theta - c) \right\} \Big/ \left\{ 1 + \left(\frac{a\sin\theta + y_c + d}{a\cos\theta - c} \right) \right\}^2$$

$$f_4' = \left\{ \left[a\cos\theta - \frac{a^2 \cos\psi_2}{\{c^2 + (d+y_c)^2\}^{1/2}} \right] \left[\frac{-a^2 \cos\psi_2 \frac{d\psi_2}{dt}}{\{c^2 + (d+y_c)^2\}^{1/2}} + \frac{a^2 \sin\psi_2 (d+y_c) \frac{dy_c}{dt}}{[c^2 + (d+y_c)^2]^{3/2}} \right] \right.$$

$$\left. - \left[a\sin\theta - \frac{a^2 \sin\psi_2}{\{c^2 + (d+y_c)^2\}^{1/2}} \right] \left[\frac{a^2 \sin\psi_2 \frac{d\psi_2}{dt}}{\{c^2 + (d+y_c)^2\}^{1/2}} + \frac{a^2 \cos\psi_2 (d+y_c) \frac{dy_c}{dt}}{[c^2 + (d+y_c)^2]^{3/2}} \right] \right\} \Big/$$

$$\left\{ \left[a\cos\theta - \frac{a^2 \cos\psi_2}{\{c^2 + (d+y_c)^2\}^{1/2}} \right]^2 + \left[a\sin\theta - \frac{a^2 \sin\psi_2}{[c^2 + (d+y_c)^2]^{1/2}} \right]^2 \right\}$$

$$\Gamma_u' = \Gamma_o N \omega_v \cos \omega_v t$$

$$\Gamma_L' = -\Gamma_o N \omega_v \cos \omega_v t$$

with $\psi_1 = \tan^{-1} \frac{(d-y_c)}{c}$

$$\psi_2 = \tan^{-1} \frac{-(d+y_c)}{c}$$

and

$$\frac{d\psi_1}{dt} = -\frac{1}{c}\frac{dy_c}{dt} \Big/ \left[1 + \left(\frac{d-y_c}{c}\right)^2\right]$$

$$\frac{d\psi_2}{dt} = -\frac{1}{c}\frac{dy_c}{dt} \Big/ \left[1 + \left(\frac{d+y_c}{c}\right)^2\right]$$

However, we are only interested in the fluctuating C_p at the Strouhal frequency. After dropping all the terms that have no Strouhal frequency components, we arrive at

$$C_p = -\frac{1}{U_0^2}\left[\frac{\Gamma_u'}{\pi}(f_1 - f_2) + \frac{\Gamma_L'}{\pi}(f_3 - f_4) + \frac{\Gamma_u}{\pi}(f_1' - f_2') + \frac{\Gamma_L}{\pi}(f_3' - f_4')\right.$$

$$\left. - 2aU_c\sin\theta\right] - \frac{4}{U_0}U_c\sin 2\theta - 2K_0\left(2\sin\theta + 4\frac{U_c}{U_0}\cos\theta\right) - K_0^2$$

$$= g \tag{16}$$

Following the scheme that was used to non-dimensionalize C_L, we change C_p into a dimensionless form. Thus

$$2a\sin\theta\frac{U_c}{U_0^2} = -\frac{\dot{Y}}{V^2}\sin(\Omega\tau + \Phi)\sin\theta$$

$$\frac{\Gamma_u'}{U_0^2} = \alpha_0\pi S N\cos\Omega\tau$$

$$\frac{\Gamma_L'}{U_0^2} = -\alpha_0\pi S N\cos\Omega\tau$$

$$\frac{\Gamma_u}{U_0^2}f_2' = \frac{\dot{Y}(\cos\theta - 2P)}{V\left[(\cos\theta - 2P)^2 + (\sin\theta + 2Y - 2H)^2\right]}$$

$$\frac{\Gamma_L}{u_0^2} f_3' = \frac{\dot{Y}(\cos\theta - 2p)}{V[(\cos\theta - 2p)^2 + (\sin\theta - 2Y - 2H)^2]}$$

$$\frac{\Gamma_L}{u_0^2} f_4' = \left[\left\{ \cos\theta - \frac{\cos\psi_2}{2[p^2 + (H+Y)^2]^{1/2}} \right\} \left\{ \frac{[\cos\psi_2\, p + \sin\psi_2\, (H+Y)]\dot{Y}}{4V[p^2 + (H+Y)^2]^{3/2}} \right\} - \left\{ \sin\theta - \frac{\sin\psi_2}{2[p^2 + (H+Y)^2]^{1/2}} \right\} \left\{ \frac{[\cos\psi_2 (H+Y) - \sin\psi_2\, p]\dot{Y}}{4V[p^2 + (H+Y)^2]^{3/2}} \right\} \right] \Bigg/ \left[\left\{ \cos\theta - \frac{\cos\psi_2}{2[p^2 + (H+Y)^2]^{1/2}} \right\}^2 + \left\{ \sin\theta - \frac{\sin\psi_2}{2[p^2 + (H+Y)^2]^{3/2}} \right\}^2 \right]$$

$$\frac{\Gamma_U}{u_0^2} f_1' = \alpha_0 (M + N \sin\Omega\tau) \left[\left\{ \cos\psi_1 \frac{p\dot{Y}}{4V[p^2 + (H-Y)^2]^{3/2}} - \frac{\sin\psi_1 (H-Y) Y}{4V[p^2 + (H-Y)^2]^{3/2}} \right\} \left\{ \cos\theta - \frac{\cos\psi_1}{2[p^2 + (H-Y)^2]^{1/2}} \right\} + \left\{ \sin\theta - \frac{\sin\psi_1}{2[p^2 + (H-Y)^2]^{1/2}} \right\} \left\{ \frac{(p\sin\psi_1 + (p-Y)\cos\psi_1)\dot{Y}}{4V[p^2 + (H-Y)^2]^{3/2}} \right\} \right] \Bigg/ \left[\left\{ \cos\theta - \frac{\cos\psi_1}{2[p^2 + (H-Y)^2]^{1/2}} \right\}^2 + \left\{ \sin\theta - \frac{\sin\psi_1}{2[p^2 + (H-Y)^2]^{1/2}} \right\}^2 \right]$$

$$K_0 = \frac{\alpha_U}{2\pi} \frac{1 - 4\{p^2 + (H-Y)^2\}}{\{1 + 4[(H-Y)^2 + p^2] - 4[\cos\theta\, p + \sin\theta\, (H-Y)]\}} - \frac{\alpha_L}{2\pi} \frac{1 - 4\{p^2 + (H+Y)^2\}}{\{1 + 4[p^2 + (H+Y)^2] - 4[\cos\theta\, p - \sin\theta\, (H+Y)]\}}$$

v) Dynamic Equation Governing the Spring-Cylinder System

The transverse motion of a rigid 2-dimensional cylinder, with viscous-type damping, mounted on linear springs is governed by the differential equation

$$m y'' + 2\beta m \omega_n y' + m \omega_n^2 y = F_y \tag{17}$$

where m is the mass per unit length, β is a measure of the damping of the system expressed in fractions of the critical damping, the level of damping above which no oscillation can take place when the system is not forced externally. ω_n is the natural frequency of the system and F_y is the external transverse force applied on the system. In the case we are considering, $F_y = L$.

A non-dimensional form of this equation is obtained by dividing thru with $2am\omega_n^2$. Thus

$$\ddot{Y} + 2\beta \dot{Y} + Y = \eta V^2 C_L \tag{18}$$

where $\eta = \frac{2a^2\rho}{m}$. Each dot represents differentiation with respect to the non-dimensional time τ once. C_L is as defined in equation (14).

Substituting equation (14) into equation (18), and after rearranging some terms we obtain

$$\ddot{Y}\left(1 + \frac{3}{2}\pi\eta\right) + Y = \eta V^2 \left[\frac{\alpha_L^2}{\pi} \frac{(Y-H)}{\{1-4[(Y-H)^2+\rho^2]\}} \right.$$

$$\left. + \frac{\alpha_L^2}{\pi} \frac{(Y+H)}{\{1-4[(Y+H)^2+\rho^2]\}} \right.$$

$$- \alpha_u \left\{ 1 - \frac{2\dot{Y}(Y-H)P + V(P^2-(Y-H)^2) - 2(Y-H)[(H-Y)^2+P^2]^{1/2} P\dot{Y}}{4V[(Y-H)^2+P^2]^2} \right\}$$

$$+ \alpha_L \left\{ 1 + \frac{2P\dot{Y}(Y+H)[(H-Y)^2+P^2]^{1/2} - 2YP(Y+H) - V[P^2-(Y+H)^2]}{4V[(Y+H)^2+P^2]} \right\}$$

$$- \frac{\dot{\alpha}_u \pi S P [\{(Y-H)^2+P^2\}^{1/2} - \frac{1}{2}]}{(Y-H)^2+P^2} + \frac{\dot{\alpha}_L \pi S P [\{(Y+H)^2+P^2\}^{1/2} - \frac{1}{2}]}{(Y+H)^2+P^2}$$

$$- \frac{\alpha_u \alpha_L (P^2+Y^2-H^2) Y}{2\pi (P^2+Y^2-H^2)+4P^2H^2} - 2\frac{\beta}{\eta V^2}\dot{Y} \Big]$$

$$= \eta f(\Omega\tau, Y, \dot{Y}) \qquad (19)$$

This equation governs the dynamics of the spring-cylinder system for a given set of parameters.

III Method of Solution

With the equations developed in II, it is possible to go ahead and solve for the pressure loading and phase and amplitude of oscillation for all velocities. However, most of the characteristics of vortex-induced oscillation are observed in the lock-in range when $\omega_v = \omega_n$. We will therefore consider only the case in the lock-in range.

i) Pressure Loading on the Cylinder

For the dynamic case being considered, we are interested in the component of fluctuating pressure at the fundamental Strouhal frequency. Theoretically, equation (16) can be decomposed into its Fourier series and the fundamental frequency can be obtained. However, this seems to be too tedious mathematically. Instead it is done numerically on the computer. Using equation (16), we can obtain the Fourier coefficients of the fundamental frequency by integration, i.e.

$$A_1 = \frac{1}{2\pi}\int_0^{2\pi} g \sin\tau \, d\tau \qquad (20A)$$

$$B_1 = \frac{1}{2\pi}\int_0^{2\pi} g \cos\tau \, d\tau \qquad (20B)$$

The root mean square value of this fluctuating pressure is given by

$$C_{p\,rms} = \frac{1}{\sqrt{2}}\left[A_1^2 + B_1^2\right]^{1/2} \qquad (20C)$$

ii) The Dynamic Equation

In equation (19), the right hand side is multiplied by the mass parameter η. This parameter is proportional to the ratio of the mass of air and the mass of the cylinder and its magnitude is of the order of $O(10^{-3})$. Therefore this equation can be solved by the small parameter approximation method in non-linear analysis. This method, the method of equivalent linearization, is explained in Appendix I. The method yields

$$Y = \bar{Y} \sin(\tau + \bar{\Phi})$$

and

$$\frac{d\bar{Y}}{d\tau} = -\frac{\bar{\lambda}}{2}\bar{Y}$$

$$\frac{d\bar{\Phi}}{d\tau} = -\frac{1}{2}\bar{K}$$

where

$$\bar{\lambda} = -\frac{\eta}{\pi\bar{Y}}\int_0^{2\pi} f(\tau, Y, \dot{Y})\cos(\tau+\bar{\Phi})\, d(\tau+\bar{\Phi})$$

$$\bar{K} = -\frac{\eta}{\pi\bar{Y}}\int_0^{2\pi} f(\tau, Y, \dot{Y})\sin(\tau+\bar{\Phi})\, d(\tau+\bar{\Phi})$$

and f is as shown in equation (19).

In the case of steady state oscillation,

$$\frac{d\bar{Y}}{d\tau} = 0 = \int_0^{2\pi} f(\tau, Y, \dot{Y})\cos(\tau+\bar{\Phi})\, d(\tau+\bar{\Phi}) \qquad (21)$$

$$\frac{d\bar{\Phi}}{d\tau} = 0 = \int_0^{2\pi} f(\tau, Y, \dot{Y})\sin(\tau+\bar{\Phi})\, d(\tau+\bar{\Phi}) \qquad (22)$$

iii) Proposed Relationship Between Amplitude and Circulation

As mentioned in II section ii, vortices in the wake are organized by the amplitude of oscillation. The phase between the formation of vortices along the spanwise direction is reduced to zero as amplitude increases to its maximum. So there is a relationship between amplitude and circulation which is to be investigated in this model. In the course of this research, various relationships between circulation and amplitude have been looked at. Obvious ones are the linear and quadratic functions. It was found that they only produced good results in parts of the lock-in range. The question, then, is what kind of relationship between amplitude and circulation the model would require for it to work in the lock-in region. By making α_o and $\bar{\Phi}$ the unknowns in the system of equations (21) and (22), the second program in Appendix II was modified to solve for these two quantities with input parameters $\bar{Y}$, M, N, P, H and v given. Guided by Feng's amplitude measurements, a function is designed relating α_o and $\bar{Y}$. This function is given by

$$
\begin{aligned}
\alpha_o = {} & .36\, e^{-79.25\left\{\frac{\bar{Y}}{\alpha_o-.1} - 1.07\right\}^2} + .06\, e^{-1089.81\left\{\frac{\bar{Y}}{\alpha_o-.1} - 1.14\right\}^2} \\
& + .06\, e^{-1089.81\left\{\frac{\bar{Y}}{\alpha_o-.1} - .1\right\}^2} + .085\, e^{-2.89\left\{\frac{\bar{Y}}{\alpha_o-.1} - 1.07\right\}^2} \\
& - .085\, e^{-35.36\left\{\frac{\bar{Y}}{\alpha_o-.1} - 1.07\right\}^2} + .018\, e^{-74.89\left\{\frac{\bar{Y}}{\alpha_o-.1} - 1.34\right\}^2} \\
& + .02\, e^{-144.46\left\{\frac{\bar{Y}}{\alpha_o-.1} - 1.25\right\}^2} - .075\, e^{-1732.87\left\{\frac{\bar{Y}}{\alpha_o-.1} - .98\right\}^2} \\
& + .224 \qquad (23)
\end{aligned}
$$

iv) Numerical Solutions

(1) Pressure Equation

The integration as indicated by equations (20A) and (20B) is carried out numerically on the IBM 360-70 computer at the computing center of UBC. The program, shown in Appendix II, uses a library routine SQUANK to perform the integration. This routine is based on Simpson's method of dividing the interval of integration into a number of divisions. The area under the curve in each of those divisions is calculated by assuming that the curve can be approximated by a quadratic. The accuracy of the value for the integral depends on the number of divisions. The routine keeps on dividing the interval into more and more divisions and comparing the result with the previous one. When the difference is smaller than an amount ϵ_1 specified by the user, the iteration will stop and the final result is obtained. In this case, ϵ_1 was specified to be .0001.

(2) Dynamic Equations

The dynamics of the cylinder-spring system are governed by equations(21), (22), and (23). These form a system of three equations in three unknowns $\bar{Y}$, Φ and α_0 . Again this system is solved by using the facilities at the computing center in

UBC. A library routine NONLIN is used to solve the system of non-linear equations. This routine is based on the Newton-Raphson method of iteration as found in (14). The first non-linear equation is expressed in a Taylor series about the initial guesses supplied by the user. Keeping only the linear terms, the resulting series is equated to zero and is solved for one variable, say x_1, in terms of the other remaining variables. In the second non-linear equation, the same procedure is applied except x_1 is replaced by the value obtained earlier. This process is repeated until in the last equation only one variable x_n is left. x_n is then solved for and back substituted into the first equation in place of the guess used. An improved x_1 is thus obtained. Then x_1 and x_n are used in the second equation to obtain an improved x_2. The process goes on until the improved solutions are calculated to within the number of significant figures specified by the user. In this case, it is set equal to 4.

IV. Analysis of Results.

Although the equations obtained are complex, the contributions of each of the quantities are clearly isolated. The values for P and H defining the position of the vortices are based on the experimental values obtained by Ferguson (13) in the Reynolds number range 1.5 - 4.1x10⁴. He determined the position of the first signal in the wake in phase with the fluctuating pressure signal on the surface of the cylinder to be at H=.47 and P=1. for the oscillating cylinder as compared with H=.5 and P=1. for the present model. Furthermore, he found that this position did not change significantly with wind speed.

The values for M and N are not based on any experimental value. They are chosen from physical arguments. In Madderom's model, he chose the values to be .5 to give good C_p distribution. This means that between the formation of the vortices in either the upper or lower row, there exists a time in which there is no vorticity at all. Physically this is not quite correct as vorticity is generated all the time at the separation point and swept downstream in the thin shear layer before it rolls up to form the discrete vortices. Thus there should be some circulation all the time in the wake and this is modelled by M being greater than N. It is found that M=.6 and N=.4 works well for this model. It might be worthwhile to point out that the elementary vortices that Gerrard (5) used in his model of the wake have mean strengths of about .682 and these oscillate at the Strouhal frequency with an amplitude of about

.502. However, one must remember this is a totally different model.

The values for β and η are .00103 and .00257 respectively. These are from the cylinder-spring system used by Feng.

The strength of circulation α_0 ranges from .22 to .58 in the lock-in region. Although it is difficult to comment on the results from a potential flow model in which there is no total head loss in the wake, it is interesting to compare this range of values with the one calculated from the data obtained by Fage and Johansen (12) at a Reynolds number of 3×10^4.

As shown in the diagram below, the rate vorticity is shed is given by

$$K = \int_0^{z_0} V_0 \frac{\partial V_0}{\partial z}\, dz = \frac{V_1^2 - V_2^2}{2}$$

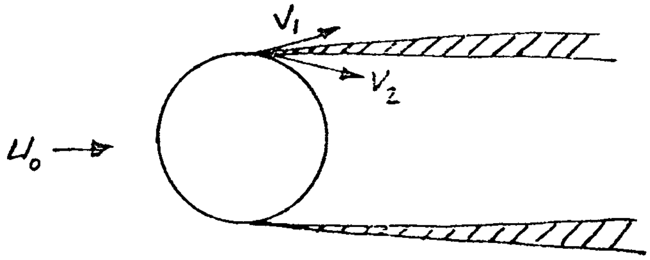

The average K is .9 and the average convection speed V_a is .757U_0 from x=0 to x=.796(2a). Now only an amount ϵ_2 of the total vorticity shed shows up in the discrete vortex. Therefore $f_v \Gamma_0 = \epsilon_2 K$. ϵ_2 was estimated to be .5. If b is the vortex spacing, $f_v = V_a/b$. This gives

$$\frac{\Gamma_0}{u_0 a} = \frac{b}{u_0 a} \epsilon_2 \frac{K_0}{V_a} = \frac{b}{a} \epsilon_2 \frac{K_0/u_0^2}{V_a/u_0} = \frac{8.54 \times .5 \times 9}{.757} = 50.7$$

where the value b/a=8.54 is from the same paper

As shown in figure 8, this model is capable of generating the jump condition in amplitude and phase observed in experiments. One thing should be pointed is that the branch of curve between B and C is unstable. Steady state oscillation in this region is impossible according to non-linear analysis. There is no surprise that the model gives amplitudes of oscillation that follow the experimental ones closely in the whole lock-in region as it is designed to do so.

Although the phase angle between excitation and oscillation does not agree very well numerically with the ones obtained by Feng, this model shows the correct trend at the first half of the lock-in range. The values in branch e-d are higher than those in a-b. This is not the trend observed in the laboratory. The range of values for Φ is not as great as the one shown in figure 3. In the model, the value for Φ is about constant at 100° as compared to the variation from zero to 190°. All the important jumps are observed at 100° in the model while it is at -100° in the measured case.

It is more interesting to examine the relationship between α_o and $\bar{Y}$. As shown in figure 7, α_o and $\bar{Y}$ are essentially related by two linear equations joined together at one end. This seems to indicate that the wake vortices are organized, or disorganized, in a linear fashion depending on wheher you go up or down along the curves. This means that the vortex filaments are aligned from their tilting position to the axis of the cylinder gradually in a linear manner. However, Feng and Koopmann both reported a sudden change in alignment which would mean a 'threshold' amplitude is required to align the vortices.

With all the parameters thus determined, the pressure distribution on the surface of the cylinder is obtained for V=.963. At this velocity, $\bar{Y}$ =.45, Φ=98°, and α_o=.455. The result is shown in figure 9. This model is able to predict the dramatic rise in pressure coefficient observed in vortex-induced oscillation. The magnitude of the RMS value at the Strouhal frequency is in the same order as those measured by Feng. However, the 'valley' at $\theta=90^{\circ}$ deviates from measured values. The cause of this valley can easily be identified to be the $4U_c \sin 2\theta / U_o$ term in equation (16). Attempts have been made to see whether this model is able to predict the right kind of pressure distribution. The best result as far as the valley is concerned is obtained with arbitrary values for the parameters as shown in figure 10. The front half is in good agreement with those measured by Feng. The back half is more than twice as high as the measured values in some places. This is to be expected because in a potential model, there is no total head loss across the shear layers. What happens in the real separated flow is part of the flow energy is used in the formation of the shear layers. The shear layers roll up to form the wake vortices alternately. These vortices account partly for the low base pressure on the cylinder.

V Future Research and Concluding Remarks

The potential model for vortex-induced oscillation presented here is able to give the jump condition in both amplitude and phase of oscillation as observed in the laboratory. It has demonstrated its ability to isolate the effects of different quantities involved in the phenomenon. It justifies future research to elucidate the phenomenon by this approach.

Much improvement of the model is required to make it satisfactory. This can probably be achieved by incorporating the fact that circulation depends on amplitude into the characteristics of the vortices, and relating the phase of oscillation to some physical quantities in the wake.

REFERENCES

(1) Naudascher, E., 'From Flow Instability to Flow-Induced Excitation', Proc. ASME, Hy 4, July 1967, 15-40.

(2) Toebes, G. H., 'Fluidelastic Features of Flow around Cylinder', Proc. Int. Res. Sem., Wind Effects on Buildings and Structures, Ottawa, 1967.

(3) Feng, C.C., 'The Measurement of Vortex Induced Effects in Flow Past Stationary and Oscillating Circular and D-section Cylinders', M.A.Sc. Thesis, U.B.C., 1968.

(4) Koopmann, G.H., 'The Vortex Wake of Vibrating Cylinders at Low Reynolds Number', JFM, 28, 3, 1969, 501-12.

(5) Gerrard, J.H., 'The 3-dimensional Structure of the Wake of a Circular Cylinder', JFM, 25, 1966, 143-164.

(6) Jordan, S.K., and Fromm, J.E., 'Oscillating Drag, Lift, and Torque on a Circular Cylinder in a Uniform Flow', Phys. Fluids, 15, 3, March, 1972, 371-6.

(7) Gerrard, J.H., 'Numerical Computation of the Magnitude and Frequency of the Lift on a Circular Cylinder', Phil. Tran. Roy. Soc., A, 261 Jan., 1967, 137-162.

(8) Abernathy, F.H. And Kronauer, R.E., 'The Formation of Vortex Streets', JFM, 13 , 1962, 1-20.

(9) McGregor, D.M., 'An Experimental Investigation of the Oscillating Pressure on a Circular Cylinder in a Uniform Stream', UTIAS TN 14, 1957.

(10) Madderom, P., 'Two Vortex Potential Model for Turbulent Flow Past Circular Cylinders', UBC ME Dept. Unpublished Note, April, 1966.

(11) Hartlen, R.T. And Currie, I.G., 'Lift-Oscillator Model of Vortex-Induced Vibration', Proc. ASCE, EM 5, Oct. 1970, 577-591.

(12) Milne-Thomson, L.M., 'Theoretical Hydrodynamics', 5th Ed., MacMillan, 1968.

(13) Ferguson, N., 'The Measurement of Wake and Surface Effects in the Sub-critical Flow Past a Circular Cylinder at Rest and in Vortex-Excited Oscillation', M.A.Sc. Thesis, UBC, 1965.

(14) Fage, A. And Johansen, F.C., 'The Structure of Vortex Sheets', Phil. Mag., Ser. 7, Vol. 5, #28, Feb. 1928, 417-441.

(15) Kryloff, N., and Bogoliuboff, N., 'Introduction to Non-Linear Mechanics', Princeton University Press, 1947.

(16) Brown, K.M., 'The Solution of Simultaneous Nonlinear Equations', Proc. ACM National Meeting, 1967, 110-114.

APPENDIX I

Method of Equivalent Linearization

We consider non-linear differential equations of the form

$$\ddot{Y} + Y = \eta f(\Omega\tau, Y, \dot{Y}) \tag{1}$$

where η is a small parameter. The external forcing function $f(\Omega\tau, Y, \dot{Y})$ can be replaced by an equivalent linear one e with an accuracy to within the order of η^2 (see reference 15). Assuming $Y = \bar{Y}\sin(\Omega\tau + \bar{\Phi})$, we put

$$e = -\bar{\lambda}\,\bar{Y}\Omega\cos(\Omega\tau + \bar{\Phi}) - \bar{K}\,\bar{Y}\sin(\Omega\tau + \bar{\Phi})$$

Comparing this with the external forcing function f, we obtain

$$\bar{\lambda} = -\frac{\eta}{\pi\bar{Y}\Omega}\int_0^{2\pi} f(\Omega\tau, Y, \dot{Y})\cos(\Omega\tau + \bar{\Phi})\, d(\Omega\tau + \bar{\Phi})$$

$$\bar{K} = -\frac{\eta}{\bar{Y}\pi}\int_0^{2\pi} f(\Omega\tau, Y, Y)\sin(\Omega\tau + \bar{\Phi})\, d(\Omega\tau + \bar{\Phi})$$

Thus equation (1) becomes

$$\dot{Y} + \bar{\lambda}\,\dot{Y} + (1 + \bar{K})\,Y = 0 \tag{2}$$

From the theory of linear oscillation, we get

$$\frac{d\bar{Y}}{d\tau} = -\frac{\bar{\lambda}}{2}\bar{Y}$$

$$\frac{d\bar{\Phi}}{d\tau} = \sqrt{1-\bar{K}} - \Omega$$

For the lock-in range, $\Omega = 1$.

$$\left.\begin{aligned} \therefore\ \frac{d\bar{\Phi}}{d\tau} &\simeq 1 - \frac{1}{2}\bar{K} - 1 = -\frac{1}{2}\bar{K} \\ \frac{d\bar{Y}}{d\tau} &= -\frac{\bar{\lambda}}{2}\bar{Y} \end{aligned}\right\} \qquad (3)$$

APPENDIX II

The following program calculates C_{prms} at Strouhal frequency.

```
      REAL M,N
      COMMON/FUN/THETA,X1,X2,ALFA,P,M,N,S,V,H,PI
      S=.2
      PI=3.14159
      READ(5,10) X1,X2,ALFA,M,N,P,H,V
 10   FORMAT(10F10.5)
      DO 123 II=1,37
      THETA=PI/18.
      THETA=THETA*(FLOAT(II)-1.)
      EXTERNAL CPSIN
      CPRMSS=SQUANK(CPSIN,.0,6.28318,.0001,TOL,FIFTH)
      EXTERNAL CPCOS
      CPRMSC=SQUANK(CPCOS,.0,6.28318,.0001,TOL,FIFTH)
      CPFUN=SQRT((CPRMSS**2+CPRMSC**2)/2./PI**2)
      ANGLE=(THETA/PI)*180.
      WRITE(6,124)          ANGLE ,CPFUN ,CPRMSS,CPRMSS,CPRMSC
 124  FORMAT(7G15.4)
 123  CONTINUE
      STOP
      END
IN EFFECT*  ID,EBCDIC,SOURCE,NOLIST,NODECK,LOAD,NOMAP
IN EFFECT*  NAME = MAIN     , LINECNT =       57
CS*    SOURCE STATEMENTS =        20,PROGRAM SIZE =      762
CS*  NO DIAGNOSTICS GENERATED
MAIN
```

```
      FUNCTION CPCOS(TAU)
      COMMON/FUN/THETA,X1,X2,ALFA,P,M,N,S,V,H,PI
      REAL M,N
      Y=X1*SIN(TAU+X2)
      YDOT=X1*COS(TAU+X2)
      PSI1=ATAN2(H-Y,P)
      PSI2=ATAN2(-H-Y,P)
      STH=SIN(THETA)
      CTH=COS(THETA)
      SS1=SIN(PSI1)
      CS1=COS(PSI1)
      SS2=SIN(PSI2)
      CS2=COS(PSI2)
      D1=P*P+(H-Y)*(H-Y)
      D2=P*P+(H+Y)*(H+Y)
      SQD1=SQRT(D1)
      SQD2=SQRT(D2)
      PSI=ATAN2(X1+H,P)
      PHI=ARSIN(.5*SIN(PSI)/SQD2)
      F11=ATAN2(STH-SS1/(2.*SQD1),CTH-CS1/(2.*SQD1))
      IF(F11.LT.0.) GO TO 125
      IF (THETA.GT.1.5*PI) GO TO 136
      F1=F11
      GO TO 128
 125  IF(THETA.LT.PHI) GO TO 126
 136  F1=F11+2.*PI
      GO TO 128
 126  F1=F11
 128  F22=ATAN2(STH+2.*Y-2.*H    ,CTH-2.*P)
      IF(F22.LT.0.) GO TO 140
      F2=F22
      GO TO 141
 140  F2=2.*PI+F22
 141  F33=ATAN2(STH+2.*Y+2.*H,CTH-2.*P)
      IF(F33.LT.0.) GO TO 150
      F3=F33
      GO TO 151
 150  F3=2.*PI+F33
 151  F44=ATAN2(STH-SS2/(2.*SQD2),CTH-CS2/(2.*SQD2))
      IF(F44.LT.0.) GO TO 165
      IF (THETA.GT.1.5*PI) GO TO 176
      F4=F44
      GO TO 180
 165  CONTINUE
 176  F4=F44+2.*PI
 180  DF1DT=(((CS1*P-SS1*(H-Y))*YDOT)*(CTH-CS1/(2.*SQD1))-(STH-SS1/(2.*S
     1QD1))*((CS1*(Y-P)-SS1*P)*YDOT))/(4.*V*D1**1.5*((CTH-CS1/(2.*SQD1))
     2**2+(STH-SS1/(2.*SQD1))**2))
      DF4DT=((CTH-CS2/(2.*SQD2))*(CS2*P+SS2*(H+Y))*YDOT-(STH-SS2/(2.*SQD
     12))                            *(CS2*(H+Y)-SS2*P)*YDOT)/(4.*V*D2**1.5*((CT
     2H-CS2/(2.*SQD2))**2+(STH-SS2/(2.*SQD2))**2))
      DF2DT=YDOT*(CTH-2.*P)/(V*((CTH-2.*P)**2+(STH+2.*Y-2.*H)**2))
      DF3DT=YDOT*(CTH-2.*P)/(V*((CTH-2.*P)**2+(STH+2.*Y+2.*H)**2))
      ALFA1=ALFA*(M+N*SIN(TAU))
      ALFA2=ALFA*(M-N*SIN(TAU))
```

```
      AL1DOT=ALFA*N*COS(TAU)
      AL2DOT=-ALFA*N*COS(TAU)
      AKOU=ALFA1*(1.-4.*D1)/(2.*PI*(1.+4.*D1-4.*(CTH*P+STH*(H-Y))))-ALFA
     12*(1.-4.*D2)/(2.*PI*(1.+4.*D2-4.*(CTH*P-STH*(H+Y))))
      CP=-AL1DOT*S*(F1-F2)-S*AL2DOT*(F3-F4)-ALFA1/PI*(DF1DT-DF2DT)-ALFA2
     1/PI*(DF3DT-DF4DT)-4.*YDOT*SIN(2.*THETA)/V+2.*AKOU*(-2.*STH-4.*YDOT
     2*CTH/V)-AKOU*AKOU-Y/(V*V)*STH
      CPCOS=CP*COS(TAU)
      RETURN
      END
 IN EFFECT*  ID,EBCDIC,SOURCE,NOLIST,NODECK,LOAD,NOMAP
 IN EFFECT*  NAME = CPCOS    , LINECNT =       57
ICS*     SOURCE STATEMENTS =         58,PROGRAM SIZE =      2728
ICS*  NO DIAGNOSTICS GENERATED
 CPCOS

GINS

ON *SOURCE* CAUSES A RETURN TO MTS.
RMINATED
```

```
      AL1DOT=ALFA*N*COS(TAU)
      AL2DOT=-ALFA*N*COS(TAU)
      AKOU=ALFA1*(1.-4.*D1)/(2.*PI*(1.+4.*D1-4.*(CTH*P+STH*(H-Y))))-ALFA
     12*(1.-4.*D2)/(2.*PI*(1.+4.*D2-4.*(CTH*P-STH*(H+Y))))
      CP=-AL1DOT*S*(F1-F2)-S*AL2DOT*(F3-F4)-ALFA1/PI*(DF1DT-DF2DT)-ALFA2
     1/PI*(DF3DT-DF4DT)-4.*YDOT*SIN(2.*THETA)/V+2.*AKOU*(-2.*STH-4.*YDOT
     2*CTH/V)-AKOU*AKOU -Y/(V*V)*STH
      CPSIN=CP*SIN(TAU)
      RETURN
      END
S IN EFFECT*  ID,EBCDIC,SOURCE,NOLIST,NODECK,LOAD,NOMAP
S IN EFFECT*  NAME = CPSIN    , LINECNT =       57
ICS*    SOURCE STATEMENTS =        58,PROGRAM SIZE =      2728
TICS*  NO DIAGNOSTICS GENERATED
 CPSIN
```

```
      FUNCTION CPSIN(TAU)
      REAL M,N
      COMMON/FUN/THETA,X1,X2,ALFA,P,M,N,S,V,H,PI
      Y=X1*SIN(TAU+X2)
      YDOT=X1*COS(TAU+X2)
      PSI1=ATAN2(H-Y,P)
      PSI2=ATAN2(-H-Y,P)
      STH=SIN(THETA)
      CTH=COS(THETA)
      SS1=SIN(PSI1)
      CS1=COS(PSI1)
      SS2=SIN(PSI2)
      CS2=COS(PSI2)
      D1=P*P+(H-Y)*(H-Y)
      D2=P*P+(H+Y)*(H+Y)
      SQD1=SQRT(D1)
      SQD2=SQRT(D2)
      PSI=ATAN2(X1+H,P)
      PHI=ARSIN(.5*SIN(PSI)/SQD2)
      F11=ATAN2(STH-SS1/(2.*SQD1),CTH-CS1/(2.*SQD1))
      IF(F11.LT.0.) GO TO 125
      IF (THETA.GT.1.5*PI) GO TO 136
      F1=F11
      GO TO 128
125   IF(THETA.LT.PHI) GO TO 126
136   F1=F11+2.*PI
      GO TO 128
126   F1=F11
128   F22=ATAN2(STH+2.*Y-2.*H     ,CTH-2.*P)
      IF(F22.LT.0.) GO TO 140
      F2=F22
      GO TO 141
140   F2=2.*PI+F22
141   F33=ATAN2(STH+2.*Y+2.*H,CTH-2.*P)
      IF(F33.LT.0.) GO TO 150
      F3=F33
      GO TO 151
150   F3=2.*PI+F33
151   F44=ATAN2(STH-SS2/(2.*SQD2),CTH-CS2/(2.*SQD2))
      IF(F44.LT.0.) GO TO 165
      IF (THETA.GT.1.5*PI) GO TO 176
      F4=F44
      GO TO 180
165   CONTINUE
176   F4=F44+2.*PI
180   DF1DT=(((CS1*P-SS1*(H-Y))*YDOT)*(CTH-CS1/(2.*SQD1))-(STH-SS1/(2.*S
     1QD1))*((CS1*(Y-P)-SS1*P)*YDOT))/(4.*V*D1**1.5*((CTH-CS1/(2.*SQD1))
     2**2+(STH-SS1/(2.*SQD1))**2))
      DF4DT=(((CTH-CS2/(2.*SQD2))*(CS2*P+SS2*(H+Y))*YDOT-(STH-SS2/(2.*SQD
     12))                    *(CS2*(H+Y)-SS2*P)*YDOT)/(4.*V*D2**1.5*((CT
     2H-CS2/(2.*SQD2))**2+(STH-SS2/(2.*SQD2))**2))
      DF2DT=YDOT*(CTH-2.*P)/(V*((CTH-2.*P)**2+(STH+2.*Y-2.*H)**2))
      DF3DT=YDOT*(CTH-2.*P)/(V*((CTH-2.*P)**2+(STH+2.*Y+2.*H)**2))
      ALFA1=ALFA*(M+N*SIN(TAU))
      ALFA2=ALFA*(M-N*SIN(TAU))
```

The following program calculates phase and amplitude of oscillation.

```
      REAL M,NN
      DIMENSION IPOINT(4,4), ISUB(4), COE(4,4),TEMP(4),PART(4), X(3)
      COMMON/Z/X1,X2,X3,H,P,PI,S,V,M,NN,BETA,RN,ALFA,HF
      N=3
      MAXIT=20
      NUMSIG=4
101   READ(5,10)M,NN,P,H,ALFA
10    FORMAT(15F8.5)
      S=.2
      BETA=.00103
      RN=.00257
      PI=3.14159
1     READ(5,10)V
      IF (V.EQ.0.) GO TO 35
      RFAD(5,10) X(1),X(2),X(3),CONTRO
      CALL NONLIN (4,MAXIT,NUMSIG,ISING,X,IPOINT,ISUB,COE,TEMP,PART)
      IF (MAXIT.EQ.20) WRITE(6,30)
      IF(ISING.EQ.0) WRITE(6,30)
      WRITE (6,20) X,MAXIT,ISING,V,M,NN,P,H ,ALFA
20    FORMAT('0 X''S ARE ',3G15.8,'# IT=',I3,'SING',I2,6F10.3)
30    FORMAT (1X,'NO CONVERGENCE')
      MAXIT=20
      IF(CONTRO.EQ.1) GO TO 101
      GO TO 1
35    STOP
      END
S IN EFFECT*  ID,EBCDIC,SOURCE,NOLIST,NODECK,LOAD,NOMAP
S IN EFFECT*  NAME = MAIN    , LINECNT =       57
TICS*    SOURCE STATEMENTS =       26,PROGRAM SIZE =     1078
TICS*  NO DIAGNOSTICS GENERATED
N MAIN
```

```
      SUBROUTINE FK(N,X,Y,K)
      COMMON/Z/X1,X2,X3,H,P,PI,S,V,M,NN,BETA,RN,ALFA,HF
      DIMENSION X(N)
      EXTERNAL F1,F2
      A=-1089.81
      B=.06
      C=-79.248
      D=1.07
      X1=X(1)
      X2=X(2)
      X3=X(3)
      RLIM=0.
      RLIMU=3.14159*2.
      GO TO (10,20,30),K
10    Y=SQUANK(F1,RLIM,RLIMU,.00001,TOL,FIFTH)
      RETURN
20    Y=SQUANK(F2,RLIM,RLIMU,.00001,TOL,FIFTH)
      RETURN
   30 Y=-X(3)+.36*EXP(C*(X(1)/(X(3)-.104)-D)**2)+B*EXP((X(1)/(X(3)-.104)
     1-1.14)**2*A)+B*EXP(A*(X(1)/(X(3)-.104)-.1)**2)+.085*EXP(-2.8929*(X
     2(1)/(X(3)-.1040)-1.07)**2)-.085*EXP(-35.3646*(X(1)/(X(3)-.104)-1.0
     37)**2)+.224+.018*EXP(-74.8933*(X(1)/(X(3)-.104)-1.34)**2)+.02*EXP(
     4-141.459*(X(1)/(X(3)-.104)-1.25)**2)-.075*EXP(-1732.87
     57*(X(1)/(X(3)-.104)-.98)**2)
      RETURN
      END
 IN EFFECT*  ID,EBCDIC,SOURCE,NOLIST,NODECK,LOAD,NOMAP
 IN EFFECT*  NAME = FK       , LINECNT =       57
ICS*     SOURCE STATEMENTS =        21,PROGRAM SIZE =      1572
ICS*  NO DIAGNOSTICS GENERATED
 FK
```

ERMINAL SYSTEM FORTRAN G(41336)   F1

```
      FUNCTION F1(TAO)
      COMMON/Z/X1,X2,X3,H,P,PI,S,V,M,NN,BETA,RN,ALFA,HF
      REAL M,NN,N
      N=NN
      TAU=TAO-X2
      ALFA1=X3*(M+N*SIN(TAU))
      ALFA2=X3*(M-N*SIN(TAU))
      Y=X1*SIN(TAU+X2)
      YDOT=X1*COS(TAU+X2)
      PS=P*P
      HS=H*H
      YS=Y*Y
      AA=(ALFA1)**2*(Y-H)/(PI*(1.-4.*((Y-H)**2+PS)))
      AB=(ALFA2)**2*(Y+H)/(PI*(1.-4.*((Y+H)**2+PS)))
      AC=ALFA1*(-1.+(2.*YDOT*(Y-H)*P+(PS-(Y-H)**2)*V-2.*(Y-H)*SQRT((H-Y)
     1**2+PS)*P*YDOT)/(V*((Y-H)**2+PS)**2*4.))
      AD=ALFA2*(1.-(2.*YDOT*P*(Y+H)+(PS-(Y+H)**2)-2.*(H+Y)*SQRT((H-Y)**2
     1+PS)*P*YDOT)/(4.*V*((Y+H)**2+PS)**2))
      AE=ALFA1*ALFA2*Y*(PS+YS-HS)/(2.*PI*((PS+YS-HS)**2+4.*HS*PS))
      AF=X3*N*COS(TAU)*PI*S*P*(SQRT((Y-H)**2+PS)-.5)/((Y-H)**2+PS)
      AG=X3*N*COS(TAU)*PI*S*P*(SQRT((Y+H)**2+PS)-.5)/((Y+H)**2+PS)
      F1=(AA+AB+AC+AD-AE-AF-AG-2.*BETA*YDOT/(RN*V*V)        )*SIN(TAU+X2)
      RETURN
      END
S IN EFFECT*  ID,EBCDIC,SOURCE,NOLIST,NODECK,LOAD,NOMAP
S IN EFFECT*  NAME = F1      , LINECNT =       57
TICS*    SOURCE STATEMENTS =        22,PROGRAM SIZE =      1400
TICS*  NO DIAGNOSTICS GENERATED
N F1
```

```
      FUNCTION F2(TAO)
      REAL M,NN,N
      COMMON/Z/X1,X2,X3,H,P,PI,S,V,M,NN,BETA,RN,ALFA,HF
      N=NN
      TAU=TAO-X2
      Y=X1*SIN(TAU+X2)
      YDOT=X1*COS(TAU+X2)
      PS=P*P
      HS=H*H
      ALFA1=X3*(M+N*SIN(TAU))
      ALFA2=X3*(M-N*SIN(TAU))
      YS=Y*Y
      AA=(ALFA1)**2*(Y-H)/(PI*(1.-4.*((Y-H)**2+PS)))
      AB=(ALFA2)**2*(Y+H)/(PI*(1.-4.*((Y+H)**2+PS)))
      AC=ALFA1*(-1.+(2.*YDOT*(Y-H)*P+(PS-(Y-H)**2)*V-2.*(Y-H)*SQRT((H-Y)
     1**2+PS)*P*YDOT)/(V*((Y-H)**2+PS)**2*4.))
      AD=ALFA2*(1.-(2.*YDOT*P*(Y+H)+(PS-(Y+H)**2)-2.*(H+Y)*SQRT((H-Y)**2
     1+PS)*P*YDOT)/(4.*V*((Y+H)**2+PS)**2))
      AE=ALFA1*ALFA2*Y*(PS+YS-HS)/(2.*PI*((PS+YS-HS)**2+4.*HS*PS))
      AF=X3*N*COS(TAU)*PI*S*P*(SQRT((Y-H)**2+PS)-.5)/((Y-H)**2+PS)
      AG=X3*N*COS(TAU)*PI*S*P*(SQRT((Y+H)**2+PS)-.5)/((Y+H)**2+PS)
      F2=(AA+AB+AC+AD-AE-AF-AG-2.*BETA*YDOT/(RN*V*V)        )*COS(TAU+X2)
      RETURN
      END
S IN EFFECT*  ID,EBCDIC,SOURCE,NOLIST,NODECK,LOAD,NOMAP
S IN EFFECT*  NAME = F2      , LINECNT =       57
TICS*    SOURCE STATEMENTS =         22,PROGRAM SIZE =     1400
TICS*  NO DIAGNOSTICS GENERATED
N F2

TS FLAGGED IN THE ABOVE COMPILATIONS.


EGINS
```

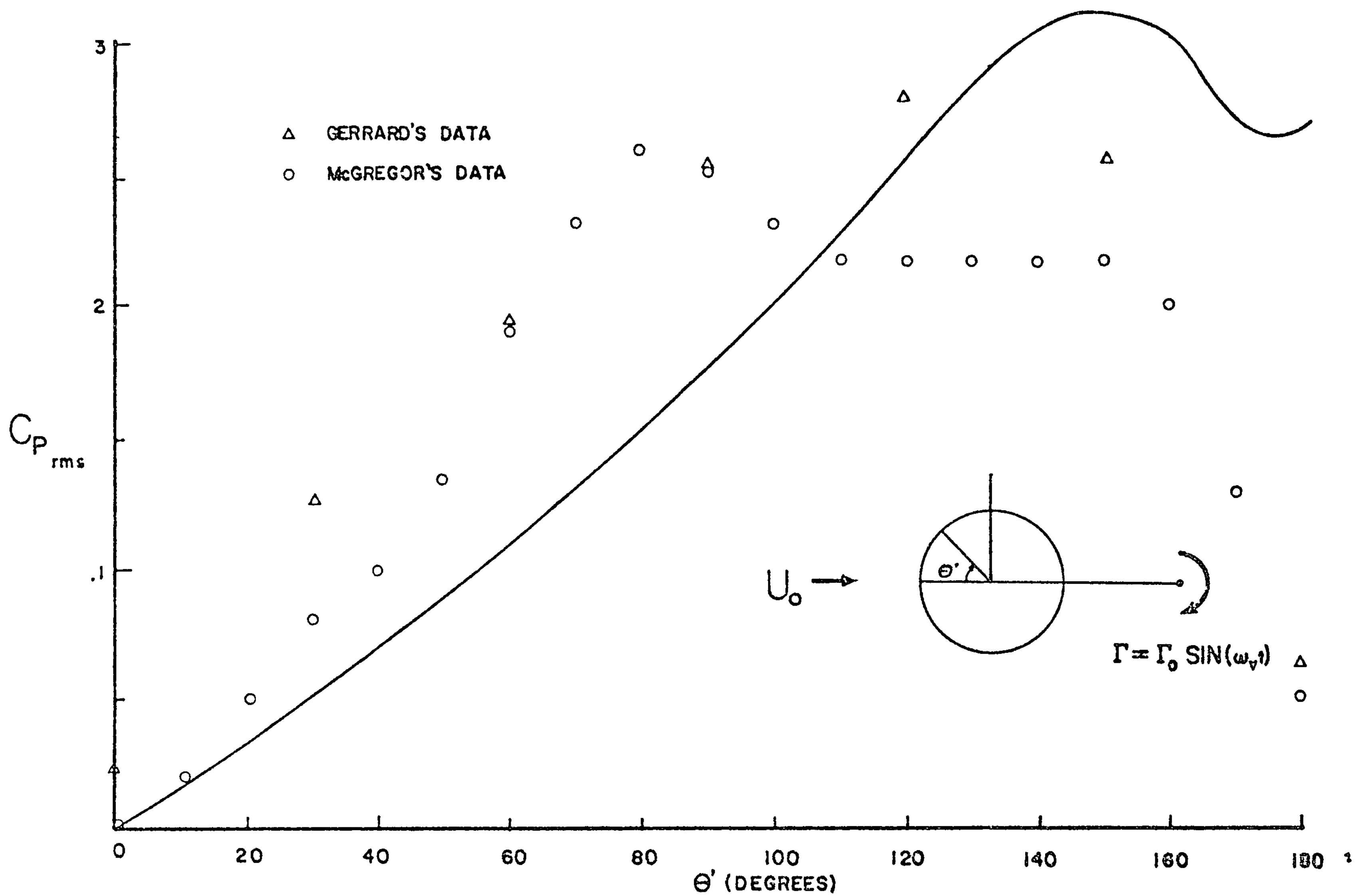

Figure 1. Single-vortex model and pressure distribution.

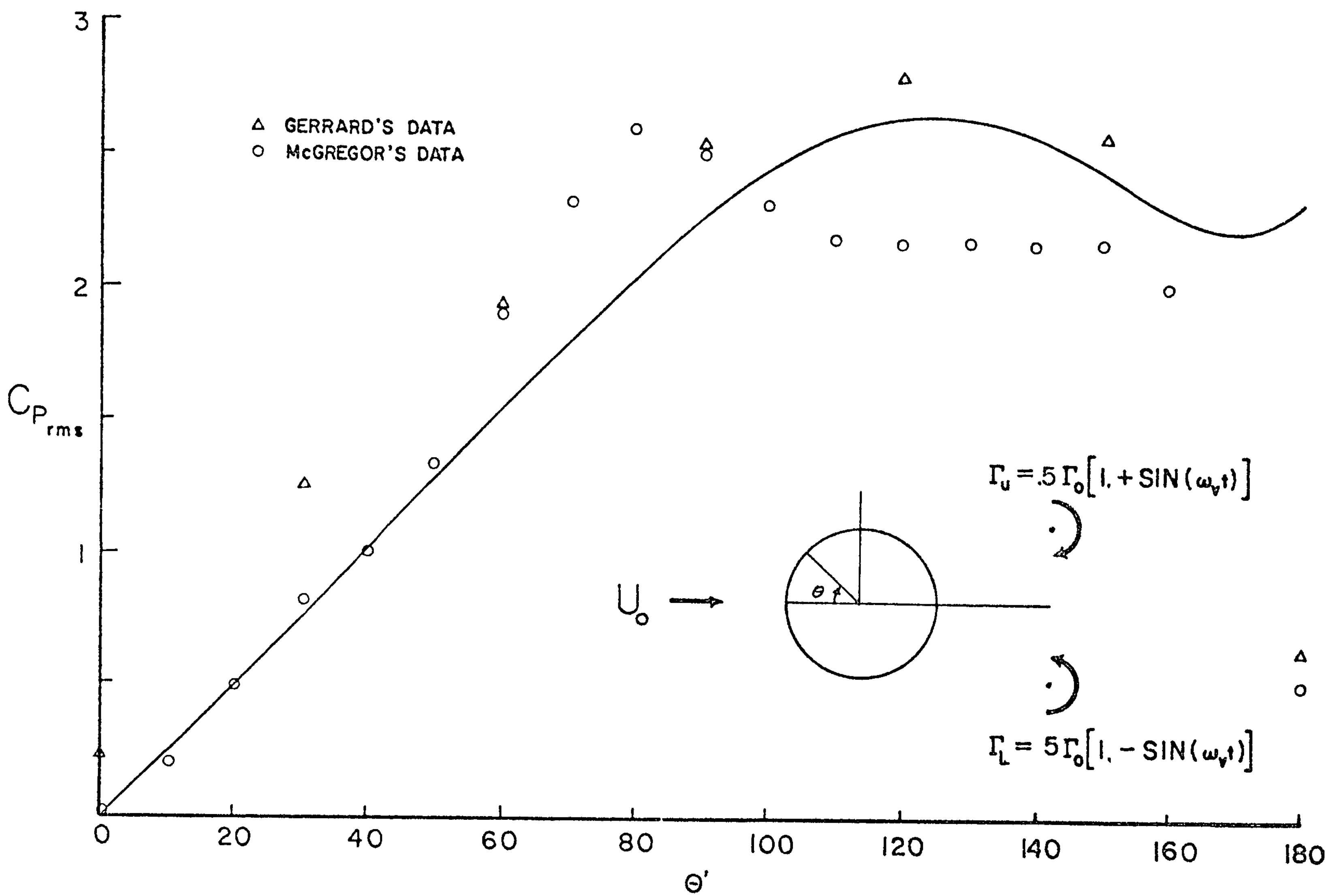

Figure 2. Two-vortex model and pressure distribution.

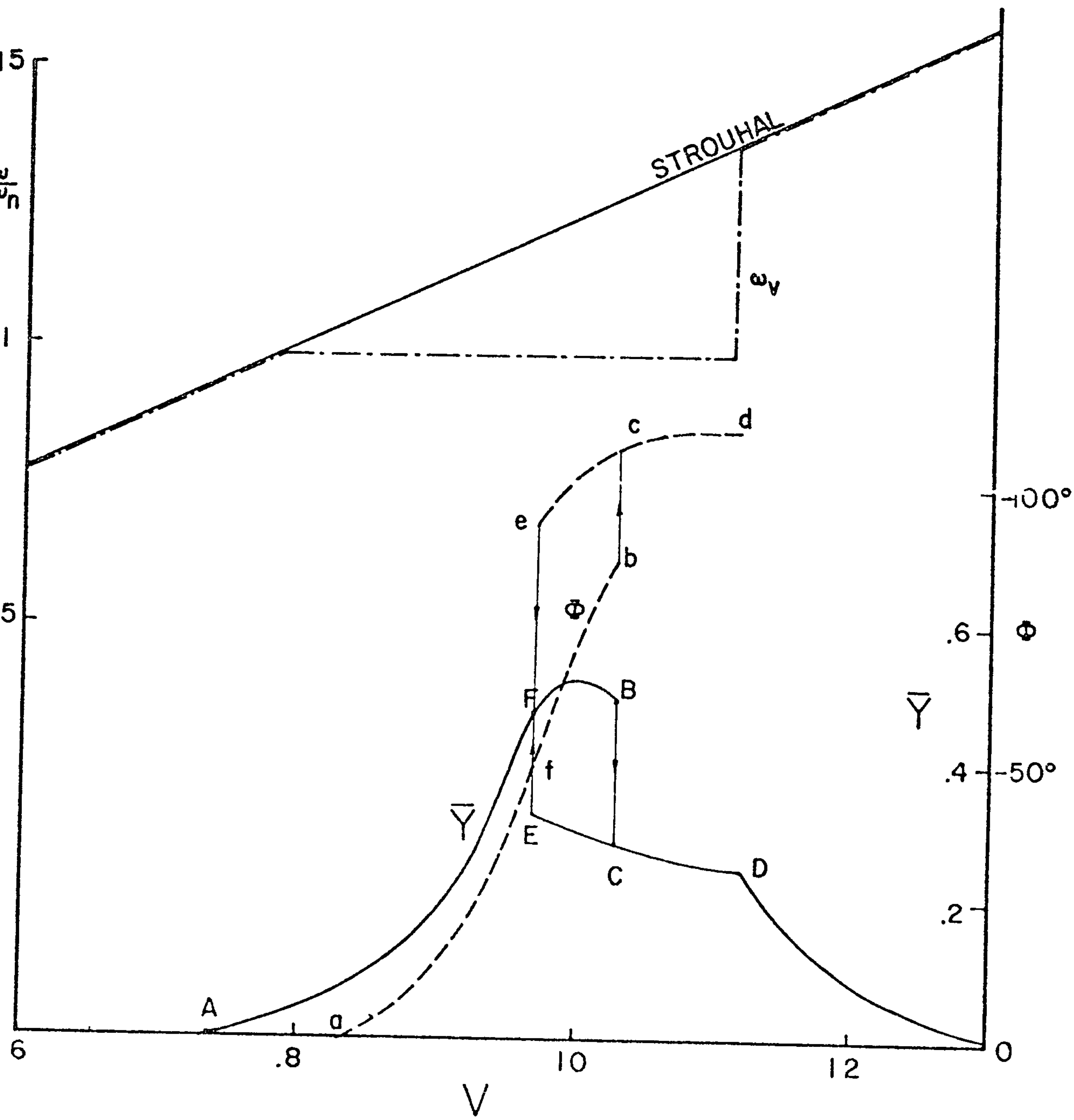

Figure 3. Vortex-induced oscillation characteristics of circular cylinder

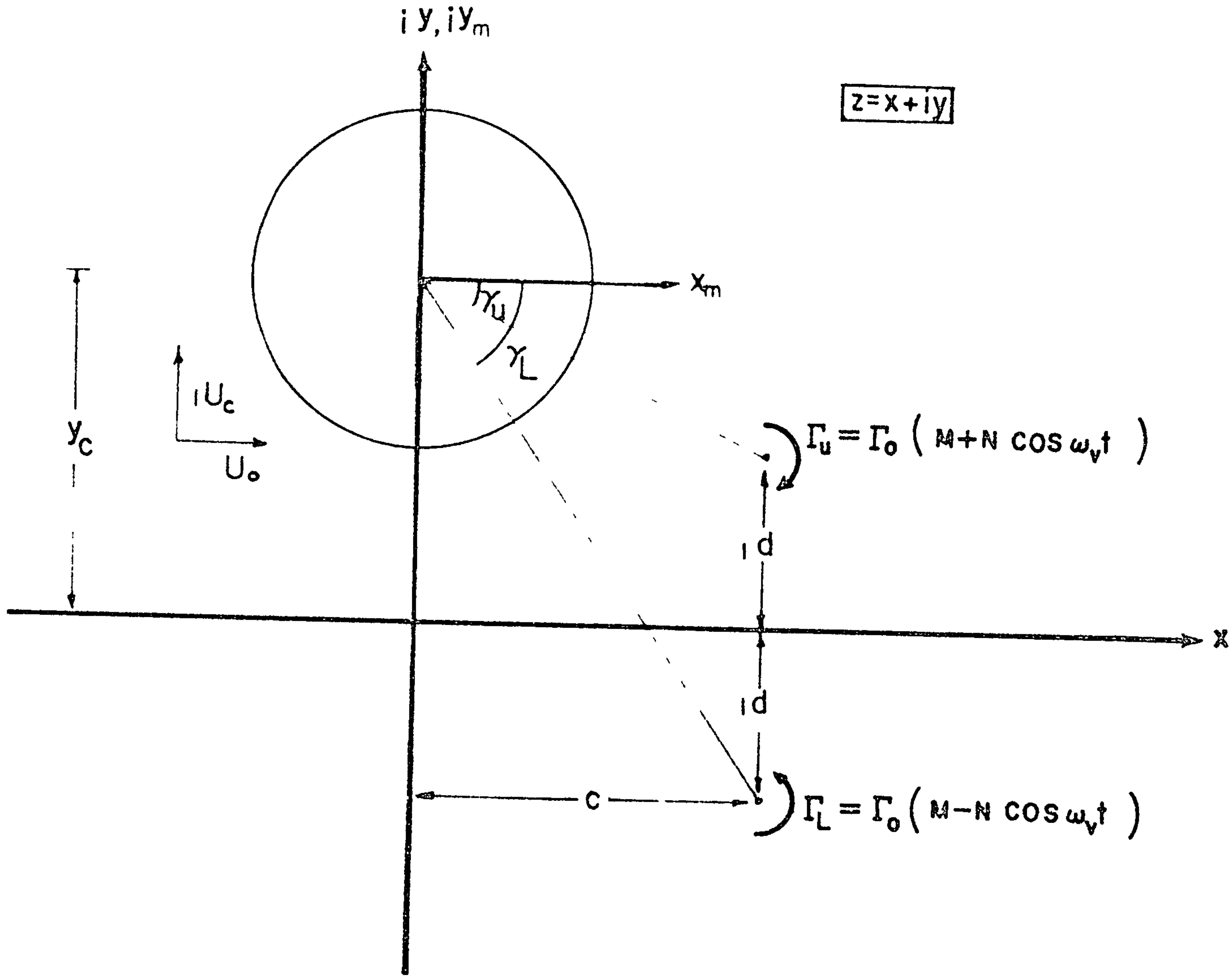

Figure 4. General set-up for the present model.

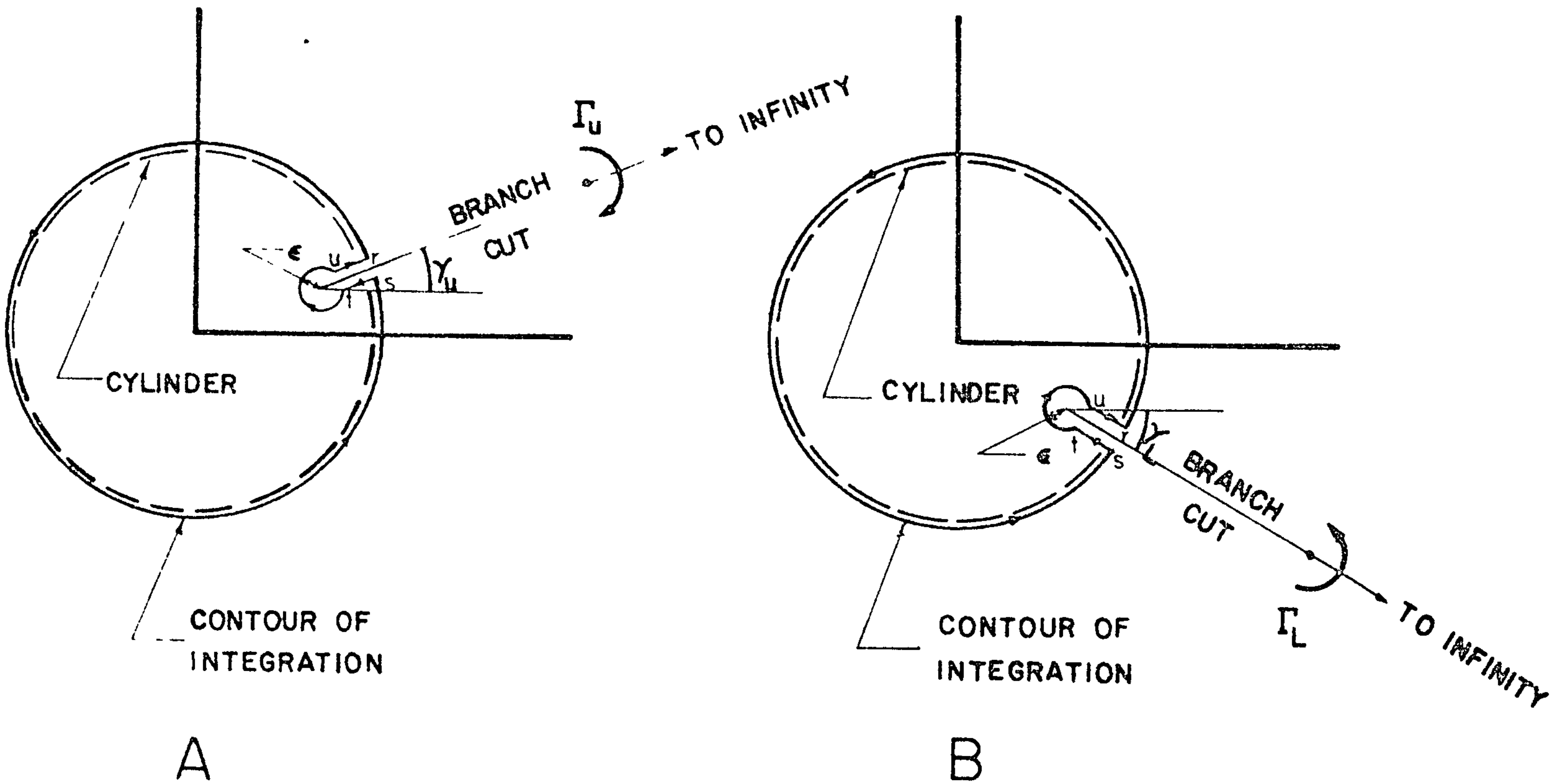

Figure 5. Contours of integration.

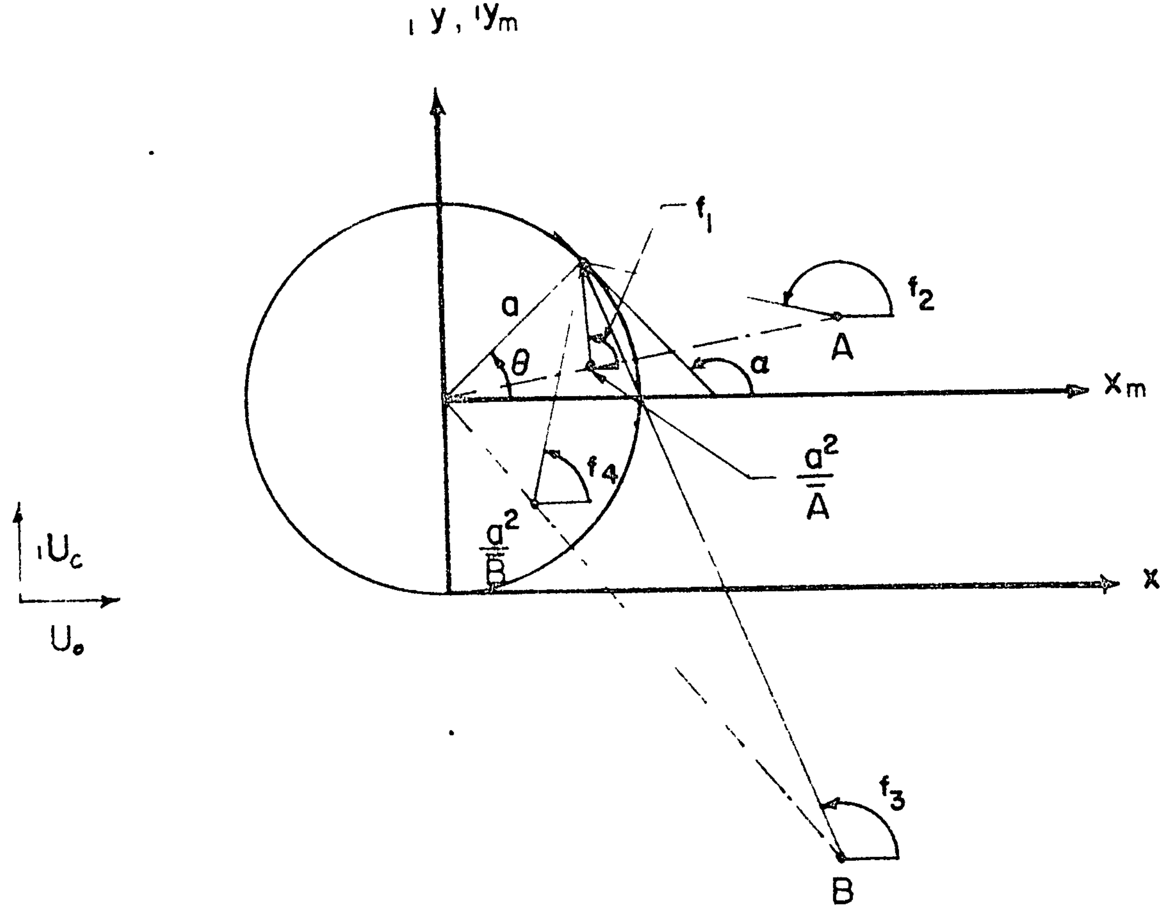

Figure 6. Notations used in the pressure equation.

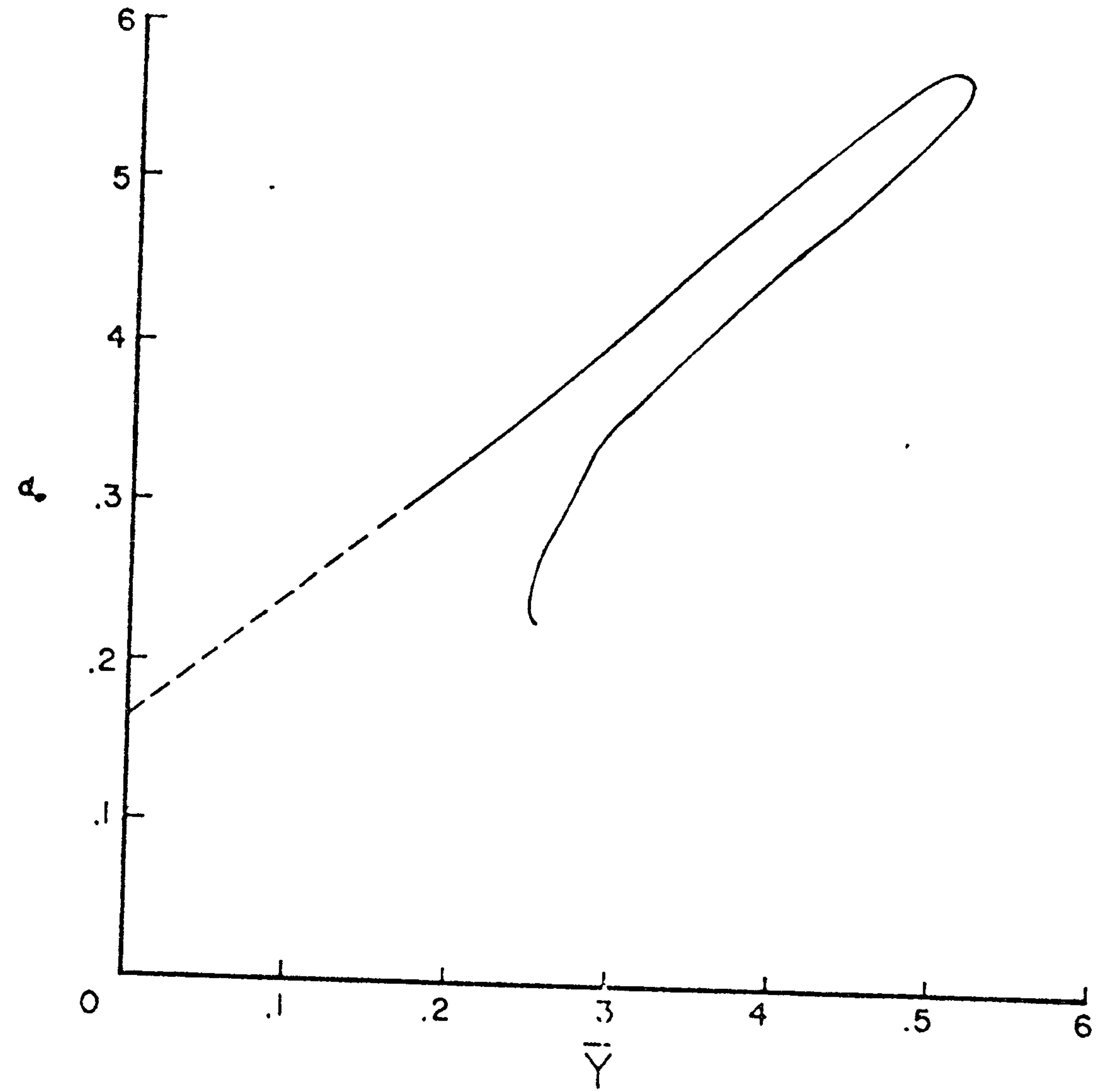

Figure 7. Proposed relationship between α_0 and $\bar{Y}$.

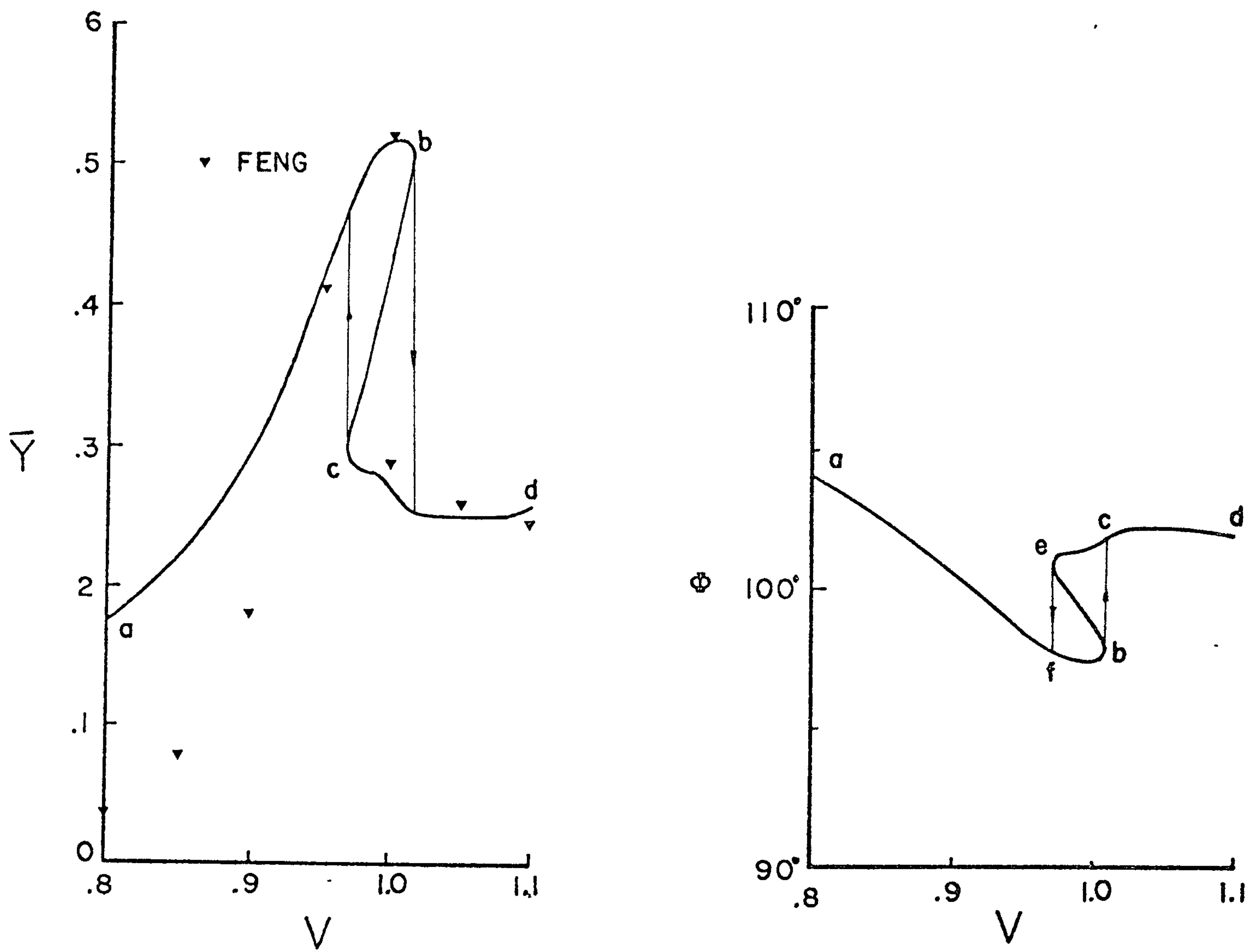

Figure 8. Phase and amplitude obtained from the present model.

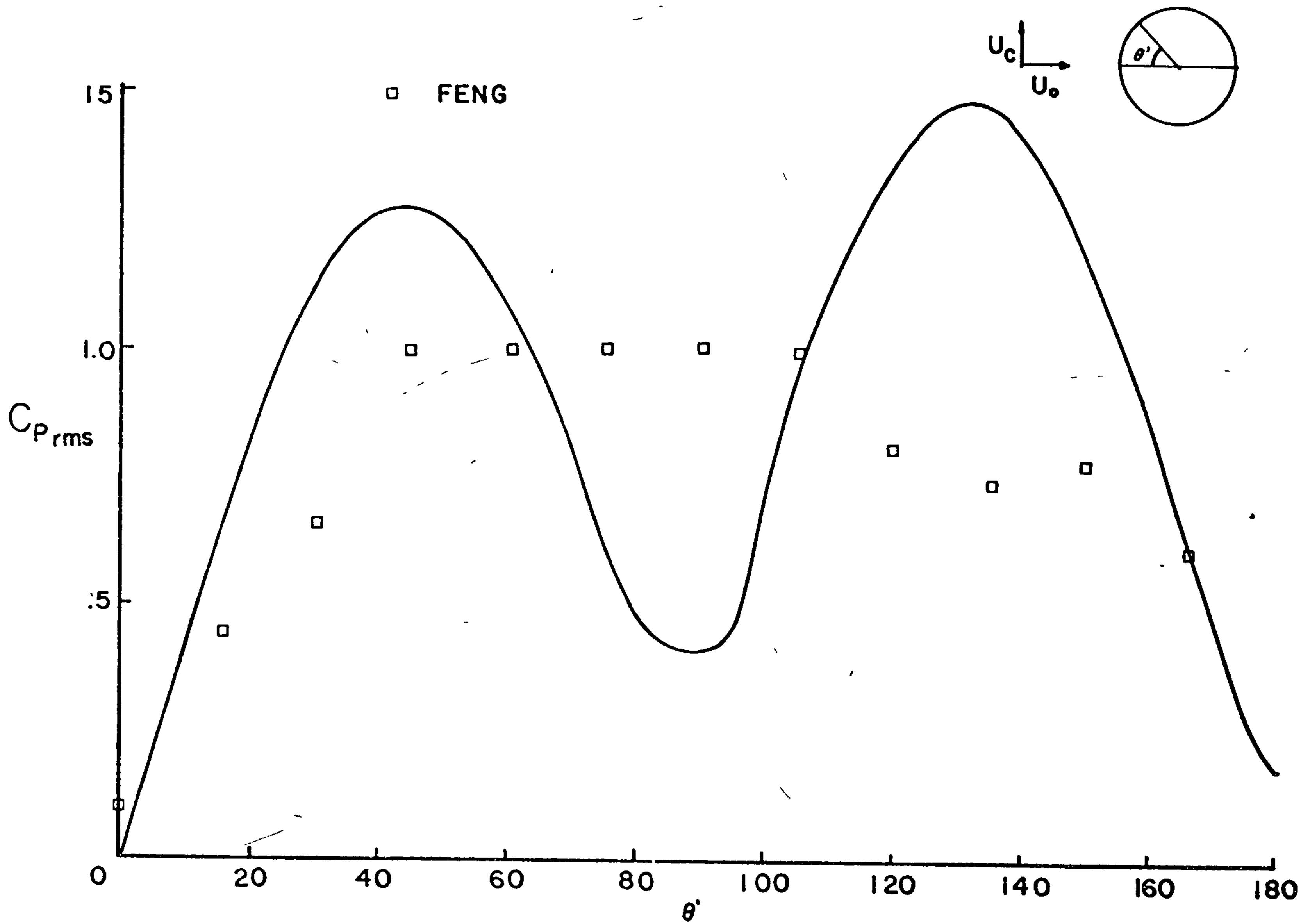

Figure 9. $C_{P_{RMS}}$ at Strouhal frequency with $V=.963$, $\bar{Y}=.46$, $\Phi=98^{\circ}$ and $\alpha_o=.55$.

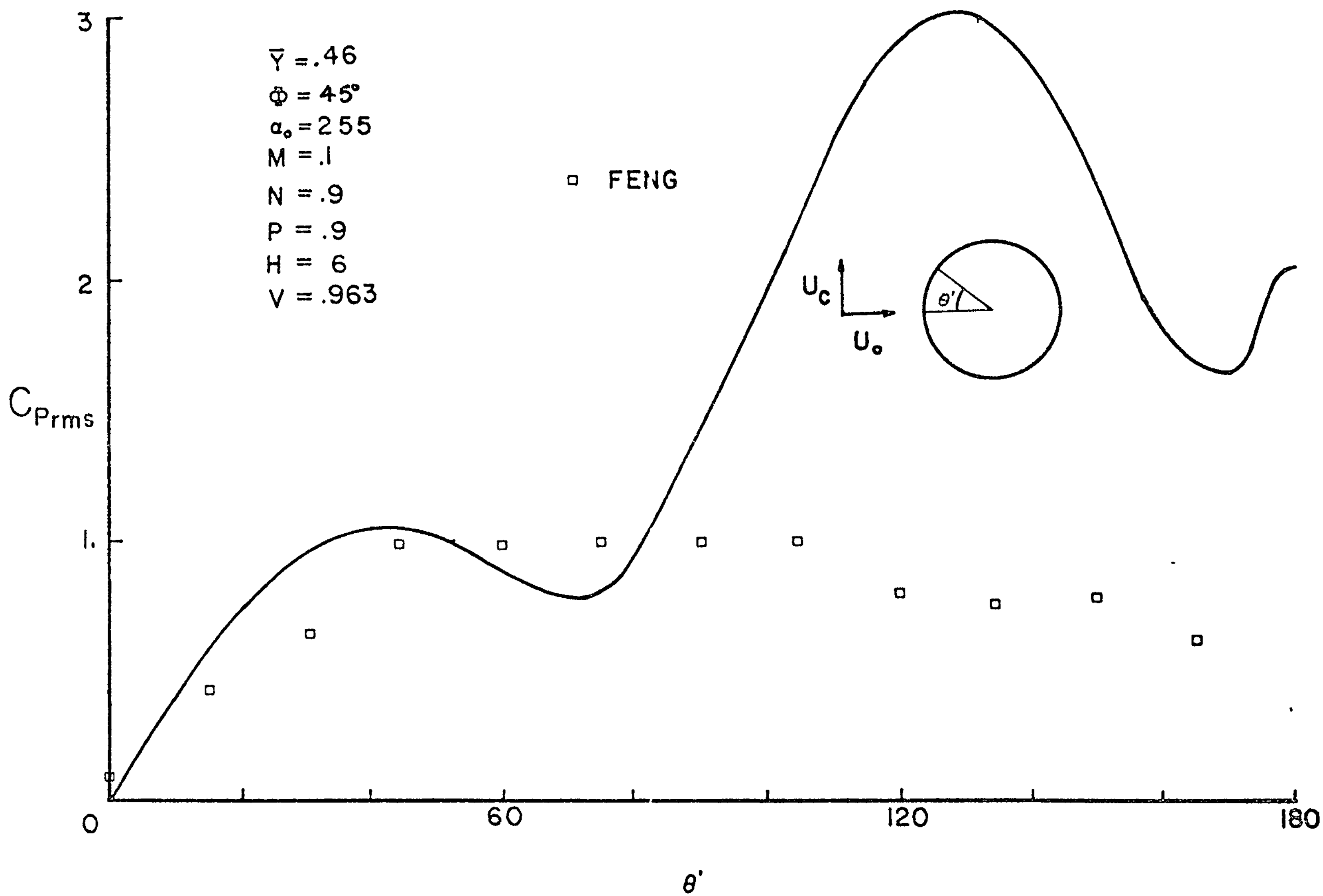

Figure 10. Comparision of C_{Prms} predicted by the present model with arbitrary values for the parameters and measured values.